

Majoritic garnet grains within shock-induced melt veins in amphibolites from the Ries impact crater suggest ultrahigh crystallization pressures between 18 and 9 GPa

Volker Stähle¹ · Rainer Altherr¹ · Lutz Nasdala² · Mario Trieloff³ · Alexander Varychev¹

Received: 25 October 2016 / Accepted: 18 September 2017 / Published online: 14 October 2017
© Springer-Verlag GmbH Germany 2017

Abstract Shock-induced melt veins in amphibolites from the Nördlinger Ries often have chemical compositions that are similar to bulk rock (i.e., basaltic), but there are other veins that are confined to chlorite-rich cracks that formed before the impact and these are poor in Ca and Na. Majoritic garnets within the shock veins show a broad chemical variation between three endmembers: (1) $\text{VIII}M^{2+}_3\text{VI}Al_2(\text{IV}SiO_4)_3$ (normal garnet, Grt), (2) $\text{VIII}M^{2+}_3\text{VI}[M^{2+}(\text{Si,Ti})](\text{IV}SiO_4)_3$ (majorite, Maj), and (3) $\text{VIII}(\text{Na}M^{2+}_2)\text{VI}[(\text{Si,Ti})Al](\text{IV}SiO_4)_3$ (Na-majorite₅₀Grt₅₀), whereby $M^{2+} = \text{Mg}^{2+}, \text{Fe}^{2+}, \text{Mn}^{2+}, \text{Ca}^{2+}$. In particular, we observed a broad variation in $\text{VI}(\text{Si,Ti})$ which ranges from 0.12 to 0.58 cations per formula unit (cpfu). All these majoritic garnets crystallized during shock pressure release at different ultrahigh pressures. Those with high $\text{VI}(\text{Si,Ti})$ (0.36–0.58 cpfu) formed at high pressures and temperatures from amphibole-rich melts, while majoritic garnets with lower $\text{VI}(\text{Si,Ti})$ of 0.12–0.27 cpfu formed at lower pressures and temperatures from chlorite-rich melts.

Furthermore, majoritic garnets with intermediate values of $\text{VI}(\text{Si,Ti})$ (0.24–0.39) crystallized from melts with intermediate contents of Ca and Na. To the best of our knowledge the ‘MORB-type’ Ca–Na-rich majoritic garnets with maximum contents of 2.99 wt% Na_2O and calculated crystallisation pressures of 16–18 GPa are the most extreme representatives ever found in terrestrial shocked materials. At the Ries, the duration of the initial contact and compression stage at the central location of impact is estimated to only ~ 0.1 s. We used a ~ 200- μm -thick shock-induced vein in a moderately shocked amphibolite to model its pressure–temperature–time (P – T – t) path. The graphic model manifests a peak temperature of ~ 2600 °C for the vein, continuum pressure lasting for ~ 0.02 s, a quench duration of ~ 0.02 s and a shock pulse of ~ 0.038 s. The small difference between the continuum pressure and the pressure of majoritic garnet crystallization underlines the usefulness of applying crystallisation pressures of majoritic garnets from metabasites for calculation of dynamic shock pressures of host rocks. Majoritic garnets of chlorite provenance, however, are not suitable for the determination of continuum pressure since they crystallized relatively late during shock release. An extraordinary glass- and majorite-bearing amphibole fragment in a shock-vein of one amphibolite documents the whole unloading path.

Communicated by Othmar Müntener.

Electronic supplementary material The online version of this article (doi:10.1007/s00410-017-1404-7) contains supplementary material, which is available to authorized users.

✉ Rainer Altherr
rainer.altherr@geow.uni-heidelberg.de

¹ Institute of Geosciences, University of Heidelberg, Im Neuenheimer Feld 234-236, 69120 Heidelberg, Germany

² Institut für Mineralogie und Kristallographie, Universität Wien, Althanstraße 14, 1090 Vienna, Austria

³ Klaus-Tschira-Labor für Kosmochemie, Institut für Geowissenschaften, Universität Heidelberg, Im Neuenheimer Feld 234-236, 69120 Heidelberg, Germany

Keywords Majoritic garnet · Shock-induced melt vein · Shock metamorphism · P – T – t conditions · Ries crater

Introduction

The suevite breccia in the Ries Crater is the famous lithotype, where a multitude of shock-related physical alterations have been observed (Stöffler et al. 2013). All the shock-induced phenomena within the crater rocks were

produced instantaneously during the passage of a supersonic compressing shock wave which originated from the central impact site of a cosmic body. The shock-metamorphic effects in meteorites and terrestrial rocks in impact craters have been recognized primarily by usage of the polarizing microscope. The observed deformational and transformational effects in the shocked rocks have been characterized with the concept of shock metamorphism (e.g., Chao 1967; French and Short 1968; von Engelhardt et al. 1970; Stöffler 1972; Stöffler et al. 1991; French and Koeberl 2010; Langenhorst and Deutsch 2012). In this context it should be mentioned that the transformation of oligoclase to jadeite and an amorphous phase (James 1969), the transformation of cordierite to diaplectic glass (Stähle 1973), the growth of kyanite along the edges of sillimanite grains (Stähle et al. 2004), the change of rutile into an α -PbO₂-structured polymorph (TiO₂II) (El Goresy et al. 2001) or into a baddeleyite-structured polymorph (akaogiite) (El Goresy et al. 2010), the modification of ilmenite into a polymorph with the Li-niobate structure (Dubrovinsky et al. 2009) and the transformation of paragonitic hornblende into a majoritic garnet (Stähle et al. 2011) were first detected in shocked rocks from the Ries crater. Recently, the newest TiO₂ mineral (riesite) formed by retrograde transformation of akaogiite was discovered (Tschauer and Ma 2017; Tschauer et al. 2017).

Shock-induced melt veins are the representatives of former thin, sheet-like appearing ultrahigh P - T melt domains, which occur in nature exclusively in shocked meteorites and terrestrial impact craters. In the last 20 years such veins obtained much attention due to the existence of distinct ultrahigh-pressure (UHP) polymorphs and new mineral species within and adjacent to these veins. The extraterrestrial samples show characteristic UHP transformations some of which are thought to happen in deeper regions of the Earth's upper mantle (e.g., Harte 2010; Liou et al. 2014; Tomioka and Miyahara 2017).

During the passage of a shock wave, certain inhomogeneities in the shock front and/or in the geometries of the target rocks produce linear shearing and frictional heating under high strain rates (Spray 1998; Langenhorst et al. 2002; Spray et al. 2004; Gillet and El Goresy 2013). This local stress leads to the formation of molten veins of varying thickness (< 2 mm). Some review articles on shock wave physics, pressure-temperature-time (P - T - t) estimations for melt veins and the occurrence of many shock-induced phase transitions in comparison with static experiments were given by Sharp and DeCarli (2006), Xie et al. (2006a, b), Gillet et al. (2007), Langenhorst and Deutsch (2012), and Gillet and El Goresy (2013). Based on petrographic observations and experimental data of static experiments we design a simplified model to estimate P - T - t conditions for the shock veins in the studied Ries amphibolites.

Contrary to chondritic and other meteorites, typical shock-induced veins have only been described from a handful of terrestrial craters. Examples are known from Vredefort (Martini 1978, 1991; Spray 1998), Rochechouart (e.g., Lambert 1981, 2010; Spray et al. 1998), Manicouagan (Langenhorst and Dressler 2003; Biren and Spray 2011), the Ries (Stähle et al. 2011) and lastly from the Canadian Steen River impact structure (Walton et al. 2016). The studied impact-induced veins from the Ries crater material show thicknesses of up to 1.1 mm and were formerly described as 'pseudotachylitic veins' (Dressler and Graup 1970; Stähle et al. 2011). Stronger shocked rocks from the Ries are totally lacking impact veins.

Many shock veins from the Ries have matrix masses that contain micrometer-sized majoritic garnets (Stähle et al. 2011). Formation of majoritic garnet reflects increasing solubility of pyroxene into the garnet structure (Ringwood 1967). In Na- and Ca-poor ultramafic systems, the classical majorite substitution is $2 \text{VI Al}^{3+} = \text{VI}(\text{Si}, \text{Ti})^{4+} + \text{VI M}^{2+}$, whereby M^{2+} represents divalent cations such as Mg^{2+} , Fe^{2+} , Ca^{2+} and Mn^{2+} . This substitution starts at ~ 6 GPa and increases with increasing pressure (Ringwood 1967; Akaogi and Akimoto 1977; Irifune 1987). According to this substitution, the chemical composition of the studied UHP garnets from the Ries revealed high crystallisation pressures in the range of ~ 15 – 17 GPa (Stähle et al. 2011). However, there exists a second coupled substitution mechanism, $\text{VIII M}^{2+} + \text{VI Al}^{3+} = \text{VIII Na}^{+} + \text{VI}(\text{Si}^{4+}, \text{Ti}^{4+})$ (Ringwood and Major 1971; Ono and Yasuda 1996; Bobrov et al. 2008, 2009; Bindi et al. 2011; Dymshits et al. 2013; Kiseeva et al. 2016) that was not taken into account by Stähle et al. (2011). In fact, this mechanism plays an important role in mafic rock compositions that often contain relatively high amounts of Na in marked contrast to peridotitic or chondritic systems. In the meantime, new means for estimating crystallization pressures of majoritic garnets in natural samples have been established (Collerson et al. 2010; Wijbrans et al. 2016).

In this paper, new data on occurrences of majoritic garnet from the Ries are given. Together with the data of Stähle et al. (2011) we are now able to better evaluate the transient shock conditions of the veins and host rocks and to give more information on the compositional relationship between majoritic garnets and the melts from which these garnets crystallized at some stage of the post-impact pressure release and cooling.

Geological setting

The circular ~ 25 -km-wide Ries crater in Southern Germany represents a medium-sized impact structure that is clearly visible in the hilly landscape. Its formation age of ~ 14.8 Ma is well established by ^{40}Ar - ^{39}Ar dating (Rocholl et al. 2011;

Buchner et al. 2013; Schwarz and Lippolt 2014). The rather young impact favoured the preservation of a thick central fall back deposit and a far-reaching ejecta blanket outside the crater. An overview on the geology of the target rocks, crater-fill and ejecta deposits, along with some geophysical data is given by Pohl et al. (1977) and Stöffler et al. (2013). The occurrence, stratigraphy and composition of all existing lithological units can be studied in detail in a number of outcrops (Schmidt-Kaler et al. 1970; Chao et al. 1978; Hüttner and Schmidt-Kaler 1999; Kenkmann and Ivanov 2006). The Variscan crystalline basement beneath the crater is mainly composed of biotite–plagioclase gneisses, amphibolites and granitic rocks (Dressler et al. 1969; Graup 1978). Additional information about the basement composition and structure comes from a 1206-m-deep research drill core ‘Nördlingen 1973’ (Stettner 1974; Graup 1977).

Analytical techniques

Some new suevite clasts containing shock veins were microscopically studied in transmitted and reflected light. Fine-grained micro-textures and mineral grains of micrometer size generally require higher magnification for reliable identification. Therefore, a great number of BSE images of domains in polished thin sections were obtained using a LEO 440 scanning electron microscope equipped with an Oxford semiconductor detector. The instrument was operated with an accelerating voltage of 20 kV and a beam current of a few nA.

Micro-Raman spectra of various small-sized mineral phases were obtained with point measurements by means of a Jobin–Yvon LabRAM-800 HR system. Spectra were obtained by excitation using the 514.5 nm emission of an Ar⁺ laser (~ 8 mW behind the objective). This confocal, notch filter-based Raman microprobe system (focal length 800 mm) was equipped with an Olympus BX41 optical microscope, a grating with 1800 grooves mm⁻¹, and a Peltier-cooled charge-coupled device (CCD) detector. With the Olympus 100× objective lens (numerical aperture 0.9), the focal spot was ~ 1 µm in diameter. The spectrometer was operated in the confocal mode; the real volume resolution is assessed to be better than 15 µm laterally and ~ 2–3 µm in depth. The wavenumber accuracy (calibrated using Ne lamp emissions) was 0.5 cm⁻¹ and the spectral resolution was 1.0 cm⁻¹. For further details see Nasdala et al. (2004).

Electron probe microanalyser (EPMA) measurements of the silicate phases were obtained using a CAMECA SX51 instrument equipped with five wavelength-dispersive spectrometers. Operating parameters were 15 kV accelerating voltage, 20 nA beam current, ~ 1 µm beam size, and counting times of 30 s for Al and Ca, 20 s for Ti and 10 s for all other elements. Natural and synthetic silicate and oxide

standards were used for calibration. Raw data were corrected for matrix effects with the PAP algorithm implemented by CAMECA. Detection limits were 0.04 wt% SiO₂, 0.06 wt% TiO₂, 0.04 wt% Al₂O₃, 0.11 wt% FeO, 0.07 wt% Cr₂O₃, 0.07 wt% MgO, 0.08 wt% MnO, 0.04 wt% CaO, 0.03 wt% Na₂O and 0.03 wt% K₂O. The total analytical error is < 1% relative.

Results

Petrography and mineral compositions

For determining the shock stage of the vein-bearing amphibolites the conventional shock classification of basaltic–gabbroic rocks from Stöffler and Grieve (2007) was used. It should be mentioned, however, that the pressures used in the basaltic–gabbroic classification at shock stage 2 are about a factor of 2 too high (Sharp and DeCarli 2006; Xie et al. 2006a; Stähle et al. 2011). This apparent discrepancy is explained in detail in the paper of El Goresy et al. (2013).

The studied shock vein-bearing amphibolites ZLN 116, ZLN 124, ZLN 128, ZLN 141, ZLN 143 and ZLN 150 were taken from the suevite of Zipplingen to the West of the Nördlinger Ries. The shocked specimens with melt veins are rare members of our voluminous Ries collection at Heidelberg. The weakly to moderately shocked clasts show light to dark greenish colors, dull lustre, and are about the size of a fist. Three polished thin sections of shocked rocks are shown in transmitted light photographs (Fig. 1). Shock veins of variable widths (1–1100 µm) cut through the shocked suevite clasts mostly without any regularity. However, the majority of the studied shock veins are only ~ 50–500 µm thick. Their contacts to the host rocks are sharp-edged. In a few cases distinct displacements along the veins are visible (Fig. 1a). The former melt bands are filled with masses of euhedral majoritic garnets and inside the fine-grained, garnetiferous matrix, there also occur rounded host minerals and rock fragments. For a petrographic description of samples ZLN 72, ZLN 86 and ZLN 100, see Stähle et al. (2011).

Amphibolite ZLN 124 with layers of leucocratic gneiss (shock stage 2a)

This sample is a unique specimen in our rock collection. It is composed of thin layers of dark-green amphibolite and leucocratic gneiss. Both layers show a weakly developed foliation running at an acute angle to the layering (Fig. 1a). A thin shock-induced vein traverses roughly at a right angle through the rock layers. A conspicuous left-lateral displacement of ~ 3.5 mm along the shock vein is highly visible and demonstrates a distinct slip (Fig. 1a). The quartz-bearing amphibolite contains many flakes

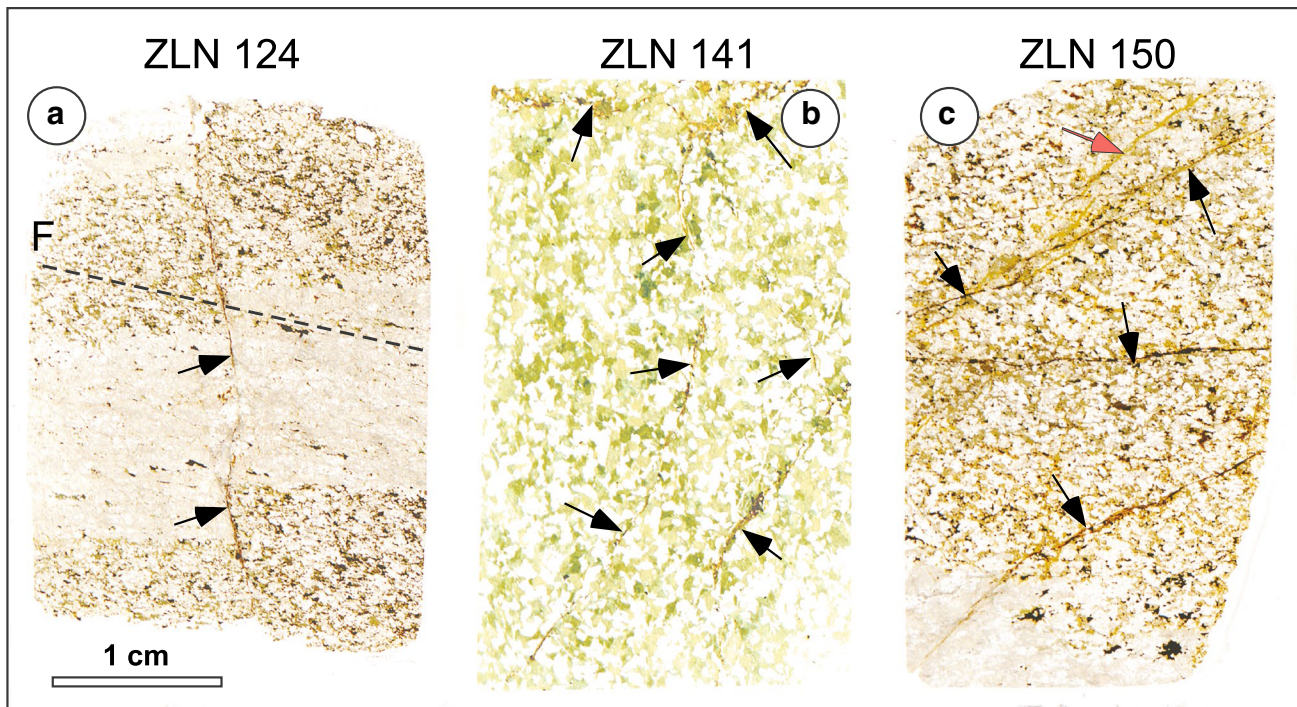


Fig. 1 Thin sections of suevite clasts containing shock-induced veins in plane polarized transmitted light. **a** Amphibolite with a layer of leucocratic gneiss (sample ZLN 124) containing a thin dark shock-induced vein (near vertical, arrows). Along this vein a left-lateral offset of ~3.5 mm is clearly visible. The foliation of this rock is marked by a black dashed line (F). **b** Amphibolite ZLN 141 with variable

thick shock-induced veins (arrows) running in different directions. **c** Quartz-bearing amphibolite (ZLN 150) with several pre-shock cracks, which are filled with yellow-green chlorite minerals. Some of these chlorite-filled fractures contain fine dark-brown colored shock-induced veins (black arrows), while others do not (red arrow). The lower bright rock section is a leucocratic gneiss

of chloritized biotite. The leucocratic gneiss is chiefly composed of strongly elongated quartz grains (“platten quartz”) and anhedral crystals of K-feldspar and plagioclase. In addition, there are single chloritized biotite and green magnesio-hornblende grains (nomenclature of amphiboles according to Hawthorne et al. 2012). Large-sized magnetite and subordinate grains of ilmenite are accessory phases.

Former plagioclase grains ($\sim \text{Ab}_{77}\text{An}_{20}\text{Or}_{03}$) in the amphibolite layers are partially isotropic and the elongated birefringent quartz grains of the gneiss are full of PDFs parallel to various crystal planes. Many PDFs are decorated giving the laminated grains a dull appearance in transmitted light. Impact-induced features classify the layered rock clast to shock stage 2a.

The thin shock-induced vein shows large variability in thickness. While it is broadest (100–250 μm) and fragment-laden inside the amphibolite layers, it is thinnest (1–20 μm) and vitreous in the leucocratic layer. As indicated by Raman spectroscopy (Fig. 3, point A), this shock vein consists of anhedral crystals of majoritic garnet. In addition, there are fragments of former quartz which are (at least partially) transformed to stishovite (Fig. 2a) as indicated by Raman spectroscopy. Inside this vein, an area with larger and

well-formed majoritic garnet grains is conspicuous (white rectangle, enlarged in Fig. 2b).

At the contact of the shock vein with the host amphibolite, an assemblage of thermally controlled phase transitions can be observed. The touching flake of a chloritized biotite (Table 1) is shock-altered to various garnetiferous grains (Fig. 2c). Close to the vein, homogeneous majoritic garnets crystallized first within the molten flake of the former chloritized biotite. More distant to the vein, non-majoritic garnet grains formed shortly after. These grains contain nanometer-sized crystals of magnetite (Fig. 2d), as confirmed by Raman spectroscopy (Fig. 3, point E). Such magnetite crystals exclusively occur within non-majoritic garnets.

The leucocratic layer of the rock (Fig. 1a) contains quartz as a main mineral constituent. When shock-induced veins cut host quartz minerals, a rather broad marginal seam (often irregular, up to 70 μm wide) of fine-grained stishovite has developed (Fig. 2e). The Raman spectrum confirms the presence of stishovite (Fig. 3, point D). Further away from the shock-vein, stishovite occupies the interstices between PDFs (arrowheads in Fig. 2e). Such a phenomenon was first described in shocked rocks from the Ries (Stähle et al. 2008). At other places, the interior of the shock-induced vein contains many quartz fragments which mostly are shock

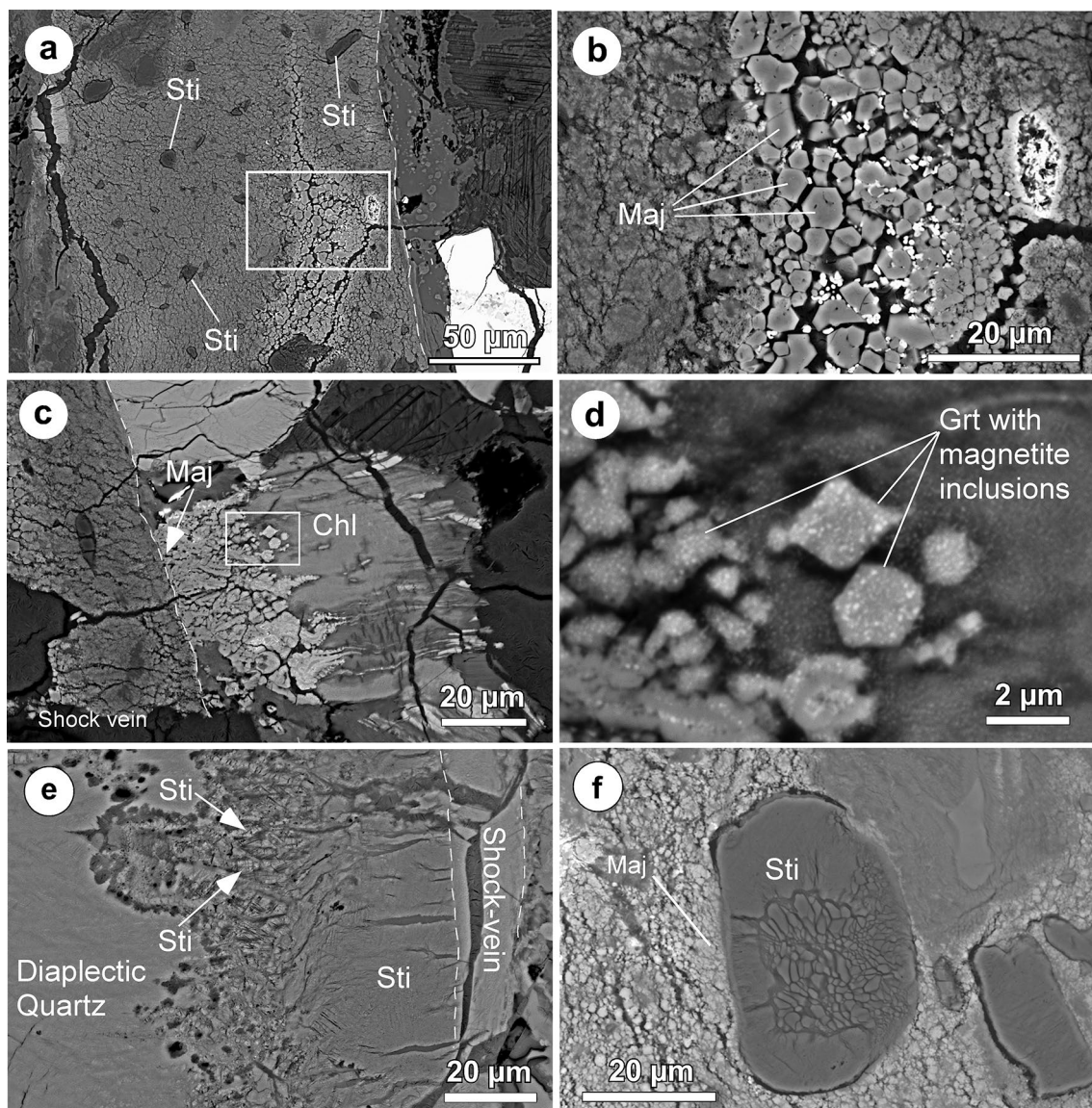


Fig. 2 Back-scattered electron (BSE) images of some areas in and adjacent to the shock-induced vein of sample ZLN 124. **a** A shock-induced vein (to the left of the white broken line) with anhedral majoritic garnet grains contains a domain with larger and brighter garnets that most likely were generated from former chlorite. **b** Larger view of the area indicated in **a**. The euhedral majoritic garnet crystals (Maj) with sizes up to 7 μm are Fe- and Mg-rich and poor in Na and Ca, suggesting a chloritic source. The small bright grains in the interspaces are very likely Fe-oxide. **c** A flake of chloritized biotite (Chl) is in contact with the shock-induced vein to the left of the broken line. Outside the vein, but direct at the contact, homogeneous majoritic garnet is formed in the former biotite grain (arrow). However, at greater distance to the contact, ‘normal’ garnets are formed (within the rectangle), reflecting a large pressure and temperature gra-

dient. **d** Detail of **c**. ‘Normal’ garnet grains (Grt) with fine-grained inclusions of magnetite (bright). The pigmented substratum around the garnets is molten chlorite with (?) spinel precipitates. **e** Diaplectic quartz grain in contact with a thin shock-induced vein. The contact zone, with some near-horizontal, contractual open spaces (on the left side of the vein), consists of fine-grained stishovite (Sti). Note in the midst of the picture fine-grained stishovite within the interspaces of PDFs (white arrowheads). Such a phenomenon was first described in shocked rocks from the Ries (Stähle et al. 2008). Miyahara et al. (2014) confirmed this observation. **f** A former quartz grain is shock-transformed to stishovite and surrounded by fine-grained majoritic garnet (Maj). In its center, the silica grain shows typical smaller shock-transformed longish grains of stishovite. The open spaces in between (dark) are due to large volume contraction (ZLN 124)

transformed to stishovite (Fig. 2a). Such a typical larger grain of stishovite inside the vein is shown in Fig. 2f. The small anhedral stishovite grains in the interior of the larger roundish grain show typical broad interspaces that obviously

resulted from strong volume contraction during stishovite formation. Low analytical totals ~ 98 wt% are probably due to significant amounts of OH⁻ (Chung and Kagi 2002; Panero et al. 2003; Litasov et al. 2007; Liu et al. 2007).

Table 1 Electron microprobe analyses of chlorite, amphibole, melt glass, zoned garnet, and prehnite. Number of cations based on 10 oxygens and 8 OH⁻ for chlorite, 22 oxygens and 2 OH⁻ for hornblende, 12 oxygens for garnet and majoritic garnet (from hornblende), and 11 oxygens and 2 OH⁻ for prehnite

Mineral	Chl	Chl	Chl	Chl	Glass	Glass	Hbl	Maj. Grt	Grt	Grt	Prh
Character	From Bio	Opaque	Primary	Primary				From Hbl	Core	Rim	Vein
Sample	124	143	143	150	141	141	141	141	128	128	128
Analysis	19	92	93	26	70	71	72	69	06	05	02
SiO ₂	26.80	30.86	31.41	30.93	57.69	57.49	46.07	46.33	40.63	40.85	43.80
TiO ₂	0.14	0.01	0.01	0.06	2.17	2.11	1.70	1.61	0.07	0.04	0.01
Al ₂ O ₃	19.36	15.62	16.24	14.77	13.81	14.14	11.32	10.94	22.17	22.55	24.84
Cr ₂ O ₃	0.00	0.02	0.00	0.00	0.08	0.06	0.02	0.05	0.00	0.00	0.00
FeO	26.02	20.74	21.02	24.15	7.54	7.07	14.62	14.64	12.65	15.88	0.36
MnO	1.00	0.41	0.33	0.28	0.12	0.03	0.35	0.39	1.23	0.75	0.00
MgO	14.77	19.35	18.91	16.00	3.10	2.76	12.07	12.27	11.60	16.44	0.00
CaO	0.06	0.40	0.37	0.75	3.76	4.10	9.34	11.66	11.22	2.78	25.82
Na ₂ O	0.40	0.29	0.04	0.85	0.51	0.47	1.49	1.34	0.02	0.05	0.14
K ₂ O	0.08	0.27	0.14	0.12	2.06	1.90	0.73	0.37	0.01	0.01	0.01
H ₂ O	11.41	11.72	11.83	11.50	n.a.	n.a.	2.05	–	–	–	4.35
Total	100.04	99.69	100.30	99.61	90.84	90.13	99.75	99.60	99.60	99.35	99.33
Si	2.818	3.158	3.183	3.225	–	–	6.743	3.488	3.025	3.006	3.018
Ti	0.011	0.001	0.001	0.005	–	–	0.187	0.091	0.004	0.002	0.001
Al	2.399	1.884	1.940	1.816	–	–	1.952	0.971	1.937	1.955	2.018
Cr	0.000	0.002	0.000	0.000	–	–	0.002	0.003	0.000	0.000	0.000
Fe ²⁺	2.288	1.775	1.782	2.106	–	–	1.790	0.922	0.784	0.977	0.021
Mn	0.089	0.036	0.029	0.025	–	–	0.043	0.025	0.077	0.047	0.000
Mg	2.315	2.952	2.858	2.488	–	–	2.633	1.377	1.282	1.803	0.000
Ca	0.007	0.044	0.040	0.084	–	–	1.464	0.941	0.891	0.219	1.906
Na	0.082	0.058	0.007	0.212	–	–	0.421	0.196	0.003	0.007	0.019
K	0.011	0.035	0.019	0.016	–	–	0.137	0.036	0.001	0.001	0.001
Total	10.018	9.944	9.859	9.977	–	–	15.372	8.050	8.004	8.018	6.983
Mg#	0.503	0.624	0.616	0.542	0.423	0.411	0.595	0.599	0.621	0.649	–

Furthermore, minor Al₂O₃ contents (~ 0.2 wt%) confirm the existence of stishovite since quartz and coesite are not able to dissolve significant amounts of Al (e.g., Bromiley et al. 2006; Panero 2006; Liu et al. 2006, 2007).

Amphibolite ZLN 116 (shock stage 2b)

The dark-green suevite clast shows a spotted appearance, which is typical for amphibolitic rocks (Spry 1969). The size of the rounded fragment is ~ 3 cm × 5 cm. The fine- to medium-grained rock shows a poorly developed foliation and a diablastic to granoblastic texture. The fine- to medium-grained rock is composed of plagioclase (~ Ab₅₀An₄₉Or₀₁), semihedral crystals of dark green pargasitic magnesio-hornblende and minor mechanically twinned clinopyroxene that is partially replaced by amphibole. Some smaller grains of apatite, ilmenite and magnetite exist. Hornblende is heavily fractured. Due to accessory grains of quartz with various sets of PDFs and the presence of isotropic, diaplectic

plagioclase glasses the adequate classification belongs to shock stage 2b (Stöffler and Grieve 2007).

Various thin, nearly opaque shock-induced melt veins inside the amphibolite clast show a complex distribution pattern. Several small branches of the vein are interconnected with a broader, main streak. They form planar to slightly curved veinlets and are 20–250 μm thick. Any contact with the host rock is razor-sharp. Careful inspection reveals that most veins follow pre-existing cracks, which were secondarily (but before the impact) filled with fine-grained chloritic material. A striking feature is seen in transmitted light with the existence of small reddish seams within the chlorite substratum on both sides of the shock vein.

High-magnification back-scattered electron (BSE) images uncover the interior of the non-transparent shock veins. Small mineral fragments of the host rock are only present in the broadest parts of the vein, while smaller sections of the veins are filled with masses of tiny grains

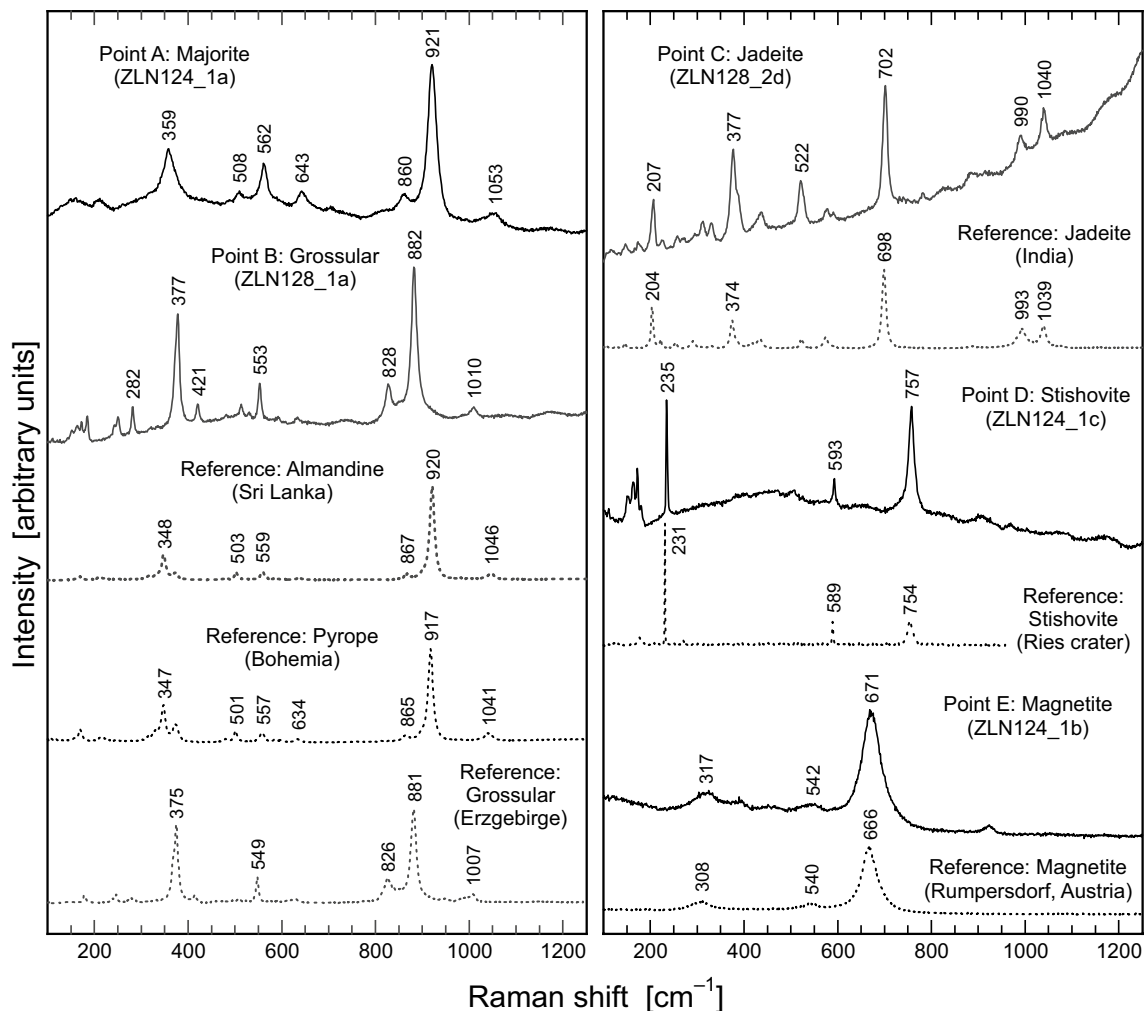


Fig. 3 Raman spectra of impact metamorphic phases and related reference samples. The spectrum of point A characterizes majoritic garnet in the shock-induced vein of ZLN 124. Grossular garnet adjacent to the shock-induced vein in ZLN 128 is confirmed with spectrum point B. Spectrum of point C results in jadeite for an assemblage of

large shock-induced grains adjacent to a shock-induced vein in sample ZLN 128. The spectrum at point D verifies stishovite at the edge of a quartz grain in contact with a shock-induced vein in sample ZLN 124. The spectrum of point E is indicative of magnetite precipitates in garnet of sample ZLN 124

of majoritic garnet. The isometric crystals reveal two different shapes. Usually, the grains show four- to six-sided straight boundaries (Fig. 4a). These polygonal outlines identify them as cubic rhombic dodecahedron. The second textural type of majoritic garnet forms dendritic individuals (Fig. 4b) documenting rapid growth and demonstrating fast quenching of the vein materials (Spry 1969). Some of the garnetiferous areas contain tiny grains (< 400 nm) of an Fe-rich oxide phase (Fig. 4a, b). Due to the small grain size of these crystals, we were not able to get reliable analyses of this Fe-rich phase. Interstices between majoritic garnets are often filled with post-shock montmorillonite minerals that formed from former glass during weathering or hydrothermal activity (Fig. 4a, b).

Amphibolite ZLN 141 (shock stage 2b)

The non-foliated amphibolite clast (Fig. 1b) is mainly composed of pargasitic magnesio-hornblende (~ 55 vol%) and plagioclase (~ 44 vol%). Plagioclase grains (~ $Ab_{50}An_{48}Or_{02}$) appear cloudy due to wholly penetration with tiny sericite flakes. In the shock-induced veins all feldspars are transformed to diaplectic glass and, with the coexistence of heavily shattered hornblende the rock refers to shock stage 2b. Several thin pre-shock veins (~ 60–100 μm wide) of colorless analcime run through this rock.

Two branches of dark brownish shock-induced veins traverse the basic rock (Fig. 1b, arrows). Both veins flow into a horizontal vein (at the top of Fig. 1b). The melt vein on the left side runs in part parallel to one of the analcime threads.

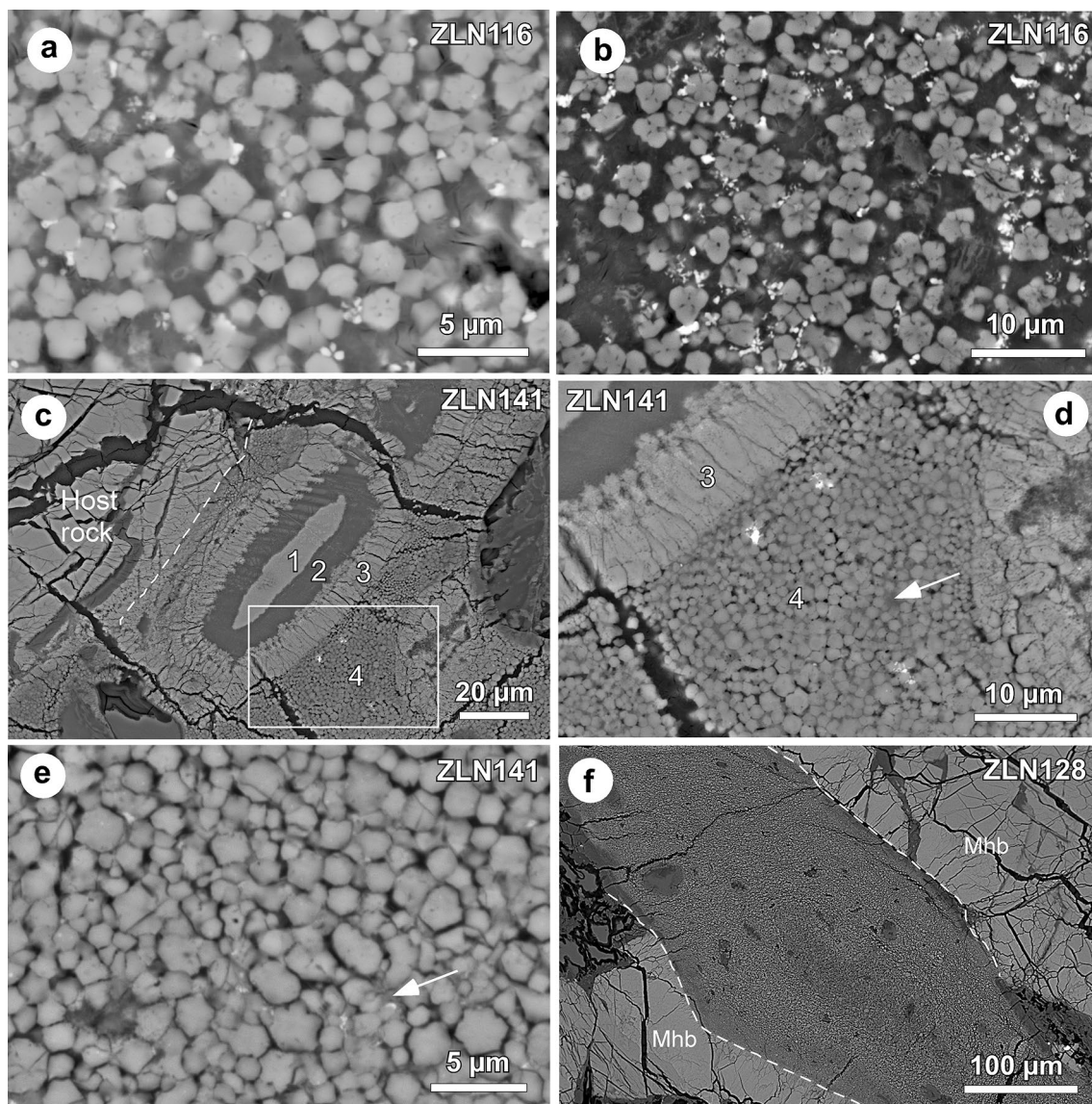


Fig. 4 BSE images of details in samples ZLN 116, 141 and 128. **a** Assemblage of equant majoritic garnets ($\sim 1\text{--}2.5\ \mu\text{m}$ in size). The small bright grains of nano-size could not be determined but seem to be iron oxides, as indicated by results of EPMA analyses. The medium grey interstices between the garnets are filled with secondary montmorillonite minerals, probably formed from glass. **b** Clusters of majoritic garnet with small open spaces in between. Dendritic crystal forms document rapid growth. The small bright grains of nano-size are probably iron oxide. Interspaces of the garnet clusters are secondarily filled with montmorillonite. **c** The oval fragment in the center of the image is a shock-transformed piece of pargasitic magnesio-hornblende (1–3) surrounded by a zone of fine-grained isometric crystals of majoritic garnet (4) within the shock vein. The residual original amphibole in the center (1) is surrounded by a dark glassy interspace (2) and a zone of majoritic garnet (3). Border between host

rock and shock vein is given by a dashed line. The rectangle gives the outlines of **d**. **d** Detail of **c** with typical accumulation of semi-hedral to euhedral majoritic garnets (4) and the edge of an amphibole fragment transformed to majoritic garnet (3). The latter shows an inner thin zone (2 μm) of more or less isolated dendritic crystals of majoritic garnet which is followed by a broader outer zone of radially oriented longish crystals of majoritic garnet. The arrow in zone (4) points to relict interstitial glass between the grains of majoritic garnet. **e** Typical accumulation of semi-hedral to euhedral majoritic garnets of $< 3\ \mu\text{m}$ in size. Arrow marks relict glassy material in between the majoritic garnet grains. **f** A typical, $\sim 200\text{-}\mu\text{m}$ -wide shock-induced vein with majoritic garnets (top left to bottom right) in sample ZLN 128. The vein passes through pargasitic magnesio-hornblende (Mhb). Note the small $\sim 10\text{-}\mu\text{m}$ -thick fine-grained “glassy” contact zones on both sides of the vein

The shock-induced melt vein and the analcite thread come together at various places, where both incorporate some components of the Na- and Si-rich zeolite material diluting

the mafic melts. The thickest shock vein, with a maximum transverse section of $\sim 500\ \mu\text{m}$ can be seen on the lower right-hand side of Fig. 1b (arrow). Inside the shock vein

numerous rounded hornblende and feldspar fragments of the host rock are assembled. These mineral enclosures are surrounded by masses of 1–3- μm -sized majoritic garnet crystals (Fig. 4d, e) that contain the highest sodium contents so far analyzed from terrestrial samples (e.g., no. 64 of ZLN 141; Table 2). Usually, the glassy matrix between the majoritic garnet grains is dissolved, but in rare cases the original silicate glass was preserved (arrow in Fig. 4d, e).

In the matrix of the vein, we found an unusual shock-transformed hornblende fragment (Fig. 4c, d). This fragment is zoned with residual hornblende in its core, an external ring of newly formed majoritic garnet and a glassy phase in between. The garnet ring is bipartite with a broader outer rim of radially oriented longish crystals and a thin inner rim with more or less isolated dentritic crystals very similar to those of Fig. 4b (sample ZLN 116). Low totals in electron probe microanalyses (~ 90 wt%) suggest that the glassy phase apparently contains large amounts of water (Table 1). High contents of SiO_2 , TiO_2 and K_2O point to the relative incompatibility of these elements in the structure of the majoritic garnet during shock-induced growth. Furthermore, the Mg# of the glass is significantly lower than that of the hornblende (Table 1).

Amphibolite ZLN 128 (shock stage 2b)

The medium-grained rock is a typical amphibolite with interlocking grains of greenish magnesio-hornblende and grayish white plagioclase (~ $\text{Ab}_{27}\text{An}_{72}\text{Or}_{01}$). The cloudy appearance of the feldspar grains is due to intensive sericitization. The mafic rock is moderately foliated and contains a post-Variscan, ~ 300- μm -thick vein of prehnite (Table 1) which was formed at hydrous conditions at some time before the shock event.

Hornblende grains are heavily shattered and plagioclase grains are totally shock-transformed to diaplectic glass suggesting a classification as shock stage 2b. The clast shows an irregular plexus of shock veins which are linked together. The branches display a great variability in thickness in the range of ~ 10–1000 μm . Hornblende fragments within the veins are completely transformed to majoritic garnet. At the intersection of a pre-impact prehnite vein with a shock-induced melt vein, tiny grains of grossularitic garnet were formed (Figs. 5a, 3, point B). We further observed an assemblage of jadeitic pyroxene in between the shock vein and diaplectic plagioclase glass. The prismatic, euhedral jadeite crystals have sizes up to 14 μm (Figs. 5b, 3, point C).

Adjacent to the shock vein a shock-altered composite domain (~ 400 μm × 200 μm in size) surrounded by pargasitic magnesio-hornblende occurs (Fig. 5c). This domain consists of a great number of newly formed non-majoritic garnet grains (1–8 μm) surrounded by an

unknown phyllosilicate (?). The rhombic dodecahedral garnet grains are conspicuously zoned and frequently contain magnetite precipitations at the innermost part of their rim zones (Fig. 5d). Relative to the garnet cores ($\text{Prp}_{42.3}\text{Alm}_{25.8}\text{Grs}_{29.4}\text{Sps}_{2.5}$), the outer rims show lower contents of Ca and Mn, but higher contents of Mg and Fe ($\text{Prp}_{59.2}\text{Alm}_{32.1}\text{Grs}_{7.2}\text{Sps}_{1.5}$) (Table 1).

Shock-induced veins in amphibolite ZLN 128 contain rounded fragments of pargasitic magnesio-hornblende that are generally shock-transformed to majoritic garnet (Stähle et al. 2011; Walton et al. 2016; Fig. 5e). In transmitted light, these transformations can be easily detected due to their bright orange colors. In BSE images shock-transformed magnesio-hornblende shows characteristic grated meshes of radial fissures at the edges and a network of curved cracks in the interior (Fig. 5e, f). Occasionally, the shock veins show fine glassy seams (Fig. 4f).

Amphibolite ZLN 143 (shock stage 2a)

The fine- to medium-grained amphibolite consists of interlocking grains of magnesio-hornblende, diopside and plagioclase. The granoblastic rock does not show a foliation. Frequently, formation of hornblende was related to the consumption of clinopyroxene. Plagioclase is partially sericitized and some chlorite-bearing veins are present. The opaques, mainly magnetite, are homogeneously distributed within the mafic rock and form a minor rock component. Most plagioclase grains (~ $\text{Ab}_{45}\text{An}_{54}\text{Or}_{01}$) are birefringent, but those closest to the shock-induced veins are completely isotropic and are transformed to diaplectic glass. Beyond this, irregularly fractured hornblende and some diopside grains with mechanical twins classify this rock to shock stage 2a.

Two diverging shock-induced veins with a thickness in the range of ~ 5–250 μm exist in this sample. The main majorite-bearing vein runs parallel to an older crack. The fracture is filled with fine-grained chloritic material (Table 1) which crystallized some time before the shock event (Fig. 6a). Close to the vein, a strange shock effect was observed. Viewed in transmitted light, the original chlorite was transformed to a blackish, ~ 30- μm -wide opaque seam (Table 1).

In BSE images, the shock-altered chlorite band is distinctly brighter than the original chlorite fillings next to it (Fig. 6a). Immediately at the edge of the vein, a small seam is recognizable where the original chlorite was molten (arrows in Fig. 6a). The true physical nature of this opaque contact zone is unknown. An open, ~ 20- μm -thick post-shock decompression crack accompanies the garnet-bearing shock-vein as is shown in Fig. 6a.

Table 2 Electron microprobe analyses of majoritic garnets from the Ries impact crater. Number of cations based on 12 oxygens and total iron = Fe²⁺

Sample	72	72	86	86	100	100	116	116	124	124	128	141	141	141	141	143	143	150 Chl	150 Chl
Analyses	28	42	12	24	12	14	2	28	16	8	23	38	62	63	64	95	96	2	6
Origin	MB	MB	MB	MB	MB	MB	Mix	Mix	MB	Chl	MB	MB	MB	MB	MB	Mix	Mix	Chl	Chl
SiO ₂	47.60	46.79	46.07	46.62	46.58	45.47	44.68	45.28	46.95	43.56	47.47	47.90	47.76	48.44	48.01	46.10	45.83	43.34	43.73
TiO ₂	0.76	0.90	0.62	0.54	0.94	0.71	0.10	0.39	0.80	0.29	0.54	0.56	0.85	0.75	0.77	0.19	0.37	0.42	0.22
Al ₂ O ₃	13.17	14.30	16.14	14.59	15.22	18.86	16.10	16.18	14.26	19.16	12.98	16.56	15.86	14.34	16.84	15.92	17.90	18.57	17.96
Cr ₂ O ₃	0.00	0.02	0.04	0.11	0.02	0.00	0.00	0.00	0.00	0.00	0.04	0.06	0.03	0.03	0.02	0.00	0.01	0.01	0.00
FeO	12.00	11.85	11.83	11.92	12.27	10.90	13.90	15.33	17.93	14.09	12.60	10.87	11.79	11.99	11.80	14.71	14.48	19.17	18.96
MnO	0.32	0.39	0.37	0.40	0.21	0.17	0.38	0.37	0.66	0.62	0.21	0.24	0.31	0.29	0.33	0.30	0.33	0.36	0.39
MgO	11.83	11.54	10.82	11.81	10.94	10.06	17.09	13.42	8.96	19.48	12.96	11.43	11.21	11.09	10.63	14.72	13.22	16.25	15.48
CaO	12.43	13.52	13.12	11.99	12.39	12.40	7.03	7.63	8.18	1.75	11.57	9.70	9.59	10.78	9.14	7.76	6.78	2.32	2.87
Na ₂ O	1.36	1.06	1.59	1.23	1.99	1.98	0.15	0.76	2.17	0.18	1.44	2.86	2.96	2.28	2.99	0.27	1.70	0.23	0.39
K ₂ O	0.19	0.33	0.18	0.29	0.21	0.13	0.04	0.09	0.47	0.02	0.14	0.08	0.07	0.20	0.12	0.19	0.09	0.09	0.09
Total	99.66	100.70	100.78	99.50	100.77	100.68	99.47	99.45	100.38	99.15	99.95	100.26	100.43	100.19	100.65	100.16	100.71	100.76	100.09
Si	3.519	3.436	3.377	3.451	3.417	3.309	3.287	3.357	3.512	3.171	3.502	3.472	3.476	3.542	3.476	3.376	3.354	3.181	3.233
Ti	0.042	0.050	0.034	0.030	0.052	0.039	0.006	0.022	0.045	0.016	0.030	0.031	0.046	0.041	0.042	0.011	0.020	0.023	0.012
Al	1.147	1.237	1.394	1.273	1.316	1.617	1.396	1.414	1.258	1.644	1.129	1.415	1.360	1.236	1.437	1.375	1.535	1.607	1.565
Cr	0.000	0.001	0.003	0.007	0.001	0.000	0.000	0.000	0.000	0.000	0.002	0.004	0.002	0.002	0.001	0.000	0.001	0.001	0.000
Fe ²⁺	0.742	0.728	0.725	0.738	0.752	0.663	0.855	0.950	1.122	0.858	0.777	0.659	0.718	0.733	0.715	0.901	0.881	1.176	1.172
Mn	0.020	0.024	0.023	0.025	0.013	0.011	0.024	0.023	0.042	0.038	0.013	0.015	0.019	0.018	0.020	0.019	0.021	0.022	0.025
Mg	1.303	1.264	1.183	1.303	1.197	1.091	1.874	1.484	0.999	2.114	1.426	1.235	1.216	1.209	1.148	1.607	1.433	1.778	1.706
Ca	0.984	1.064	1.030	0.951	0.974	0.967	0.554	0.606	0.656	0.136	0.914	0.753	0.748	0.844	0.709	0.609	0.529	0.182	0.227
Na	0.194	0.151	0.225	0.177	0.283	0.279	0.021	0.109	0.315	0.025	0.206	0.401	0.417	0.324	0.420	0.038	0.240	0.033	0.056
K	0.018	0.031	0.017	0.027	0.020	0.012	0.004	0.008	0.044	0.002	0.013	0.007	0.007	0.018	0.011	0.018	0.009	0.009	0.008
Total	7.969	7.986	8.011	7.982	8.024	7.988	8.021	7.973	7.993	8.004	8.012	7.992	8.009	7.967	7.979	7.954	8.003	8.013	8.004
Mg#	0.637	0.635	0.620	0.638	0.614	0.622	0.687	0.610	0.471	0.711	0.647	0.652	0.629	0.623	0.616	0.641	0.619	0.602	0.593
P (W16)	17.87	16.90	16.64	16.77	17.30	15.97	11.85	13.58	17.25	8.63	17.44	17.89	18.03	18.52	17.88	13.27	13.99	9.02	10.00
P (C10)	18.77	16.77	16.90	17.07	18.96	16.41	11.64	14.14	20.71	9.63	18.80	21.25	22.01	21.21	21.67	12.94	16.04	10.12	11.14

MB crystallized from metabasaltic melts, Chl crystallized from melts rich in chlorite components, Mix crystallized from melts rich in chlorite and plagioclase components, P (W16) pressure values in GPa calculated with the barometer for metabasites from Wijbrans et al. (2016), P (C10) pressure values in GPa calculated with the barometer of Collerson et al. (2010)

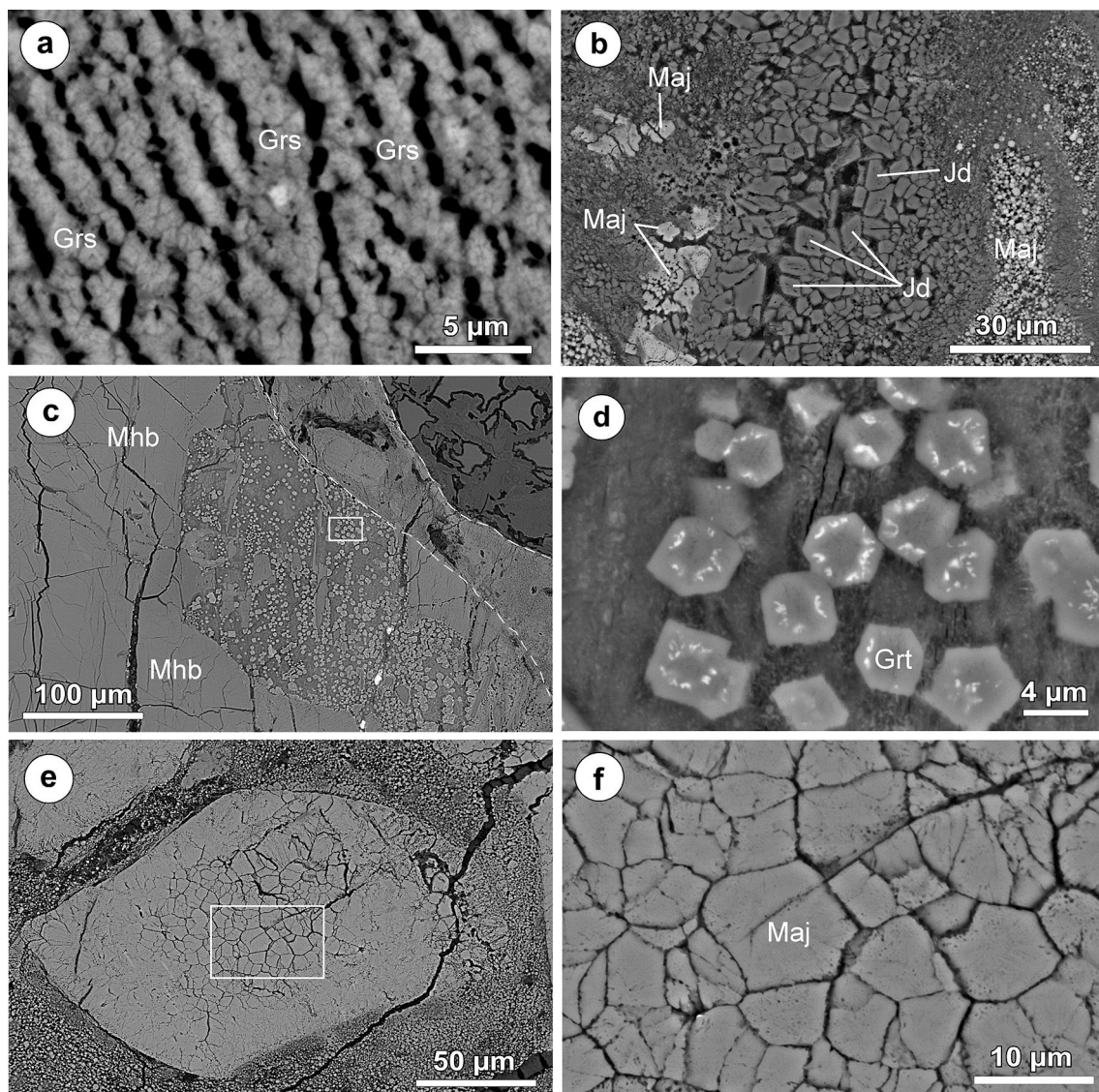


Fig. 5 BSE pictures from areas within and aside from shock-induced veins in sample ZLN 128. **a** At the intersection of a pre-impact vein filled with prehnite and a shock-induced vein, tiny grains of grossularite (Grs) have locally been formed. The black areas in between consist of secondarily dissolved glassy material. **b** Assemblage of large jadeite crystals (Jd) in the middle of the BSE picture. The bright grains are majoritic garnets (Maj). **c** A garnet-rich area neighbours on a shock-induced melt vein (between dashed lines) and paragonitic magnesian hornblende (Mhb) to the left. Beside garnet, this area consists of partially altered hornblende fragments and altered glass. **d** Detail of **c** shows some non-majoritic garnets with darker grossularite-rich cores and somewhat brighter (pyrope + almandine)-rich rims.

Quartz-rich amphibolite ZLN 150 (shock stage 2a)

Main mineral components are paragonitic magnesian hornblende, colorless diopside, transparent plagioclase ($\sim \text{Ab}_{51}\text{An}_{48}\text{Or}_{01}$) and small-sized undulatory quartz grains with PDFs. Short prismatic apatite occurs in some feldspar grains. Felsic minerals are prevailing. The quartz-bearing

The wreath of bright grains within the garnet grains consists of magnetite crystals suggesting increasing oxygen fugacities during crystal growth. **e** A large fragment of former magnesian hornblende in the shock-induced vein is completely shock-transformed to majoritic garnet. The radial fractures at the edges indicate conductive heat transfer from the melt vein and the polygonal fractures in the core formed during volume contraction. **f** Enlarged section of **e** revealing a poikilitic texture of the majoritic garnets that formed from former magnesian hornblende. The fine dark spots are very likely glassy inclusions enriched in incompatible elements like K, Ti and Si, as verified by EPMA results

amphibolite grades into a felsic feldspar- and quartz-rich gneiss layer (Fig. 1c, lower part). All quartz grains are filled with grid-shaped PDFs. Most feldspars are birefringent but some isotropic grains obviously are diaplectic plagioclase glass. Due to the established petrographic diagnostics this rock was classified to shock stage 2a.

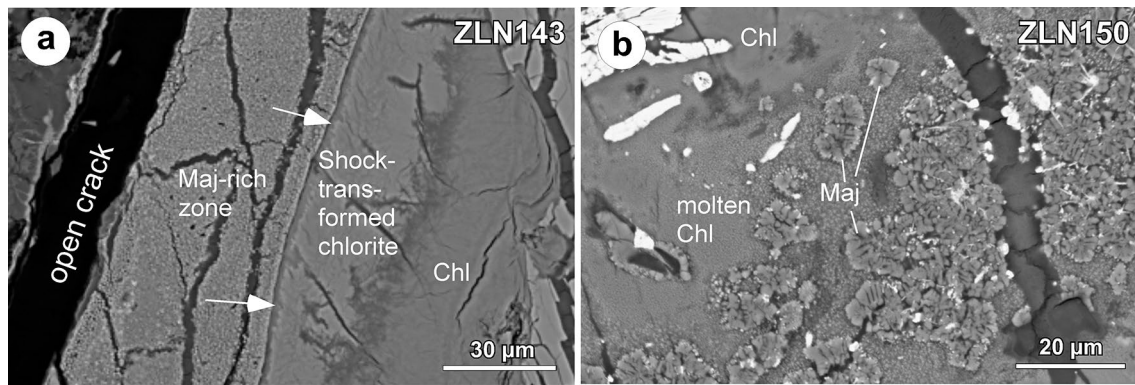


Fig. 6 BSE picture of shock-induced veins. **a** In the left-hand part of the image, a shock-induced vein full of majoritic garnet grains is visible. The dark area on the left-hand side of this zone is a post-shock open crack. To the right of the shock-induced vein, a zone of former chlorite has been altered. A thin seam ($\sim 2 \mu\text{m}$) of molten dark-grey chlorite material (arrowheads) is in contact with the shock-induced

vein. To the left, this zone is bordered by a broader zone ($\leq 30 \mu\text{m}$) of shock-transformed chlorite that merges irregularly into a zone of relict chlorite (Chl). **b** Roundish spherulitic aggregates of majoritic garnet (Maj) within molten chlorite. The fine-grained bright material within and between the majoritic spherulites is very likely a Mg–Fe spinel

Several $\sim 300\text{-}\mu\text{m}$ -wide cracks pass through the fine-grained and well-foliated amphibolite (Fig. 1c). These cracks are filled with yellow–brown chloritic material (Table 1) that crystallized at pre-shock times. Many of these pre-impact fractures contain fine, brownish opaque shock-induced melt veins ($< 80 \mu\text{m}$ wide) with majoritic garnets that either form isometric grains ($< 3 \mu\text{m}$) or spherulitic aggregates (Fig. 6b).

Chemical variability of majoritic garnet from the Ries

For EPMA analyses of majoritic garnet, we selected the largest grains ($> 2\text{--}3 \mu\text{m}$ in diameter) of each sample. Some of the results are given in Table 2 and a complete set of analyses is given in the Electronic Supplementary Material. In addition to the results on samples ZLN 116, ZLN 124, ZLN 128, ZLN 141, ZLN 143 and ZLN 150, we also use the analyses from samples ZLN 72, ZLN 86 and ZLN 100 that are given in Stähle et al. (2011). The chemical variability of majoritic garnet in the Ries reflects a continuous incorporation of the two majorite components $^{\text{VIII}}\text{M}^{2+}_3 ^{\text{VI}}[\text{M}^{2+}(\text{Si},\text{Ti})]^\text{IV}(\text{SiO}_4)_3$ and $^{\text{VIII}}(\text{NaM}^{2+}_2)^{\text{VI}}[(\text{Si},\text{Ti})\text{Al}]^\text{IV}(\text{SiO}_4)_3$ into the garnet structure. Together, these two majoritic components form between 12 and 58 mol%.

It was found that the chemical compositions of the majoritic garnets from the Ries (Table 2 and Electronic Supplementary Material) differ in a characteristic manner with regard to garnet occurrence. Those formed in shock-induced melt veins that cut both amphibole and plagioclase show higher values of $^{\text{VI}}(\text{Si} + \text{Ti})$ (0.36–0.58 cpfu) than those that were formed in veins that cut older secondary chlorite (0.12–0.27 cpfu). The first group of analyses is given by samples ZLN 72, ZLN 86, ZLN 100, ZLN 124 (nos. 11, 15, 16), ZLN 128 and ZLN 141, while the second group is represented by analyses of samples ZLN 124 (nos. 07–10) and

ZLN 150. In addition, there is a third group of samples (ZLN 116 and ZLN 143) in which we found majoritic garnets with intermediate $^{\text{VI}}(\text{Si} + \text{Ti})$ values of 0.24–0.39 cpfu. Chemical differences among the majoritic garnets become even more evident in Fig. 7a, b, where different combinations of cations are plotted versus $^{\text{IV,VI}}(\text{Si} + \text{Ti})$. In addition, these diagrams contain the two substitution lines that have been identified in majoritic garnets: (1) $2 ^{\text{VI}}\text{Al}^{3+} = ^{\text{VI}}(\text{Si},\text{Ti})^{4+} + ^{\text{VI}}\text{M}^{2+}$ (called MjEn substitution by Kiseeva et al. 2013) and (2) $^{\text{VIII}}\text{M}^{2+} + ^{\text{VI}}\text{Al}^{3+} = ^{\text{VIII}}\text{Na}^+ + ^{\text{VI}}(\text{Si}^{4+},\text{Ti}^{4+})$ (called MjJd substitution). Interestingly enough, there are substitutions that are dominated by MjEn, e.g., samples ZLN 124 Chl, ZLN 150 Chl and some analyses of sample ZLN 116, but others that are dominated by MjJd, e.g., some analyses of samples ZLN 100 and ZLN 141 (Fig. 7a, b). Most of the analyses of majoritic garnets from the Ries plot into the field between the MjEn and MjJd substitution lines, regardless of their $^{\text{IV,VI}}(\text{Si} + \text{Ti})$ values. Concerning the MjJd substitution, we state that some majoritic garnets from sample ZLN 141 show extraordinary high Na_2O contents up to 2.99 wt% (Table 2 and Electronic Supplementary Material). Majorites with Na_2O contents of 2.5–5.0 wt% were synthesized repeatedly at pressures between 17 and 27 GPa in experimental studies on N-MORB bulk compositions (references in Litasov and Ohtani 2005; Fig. 5).

In a triangular diagram of Ca–Mg–(Fe + Mn) (cpfu) the majoritic garnets of each sample plot into different fields (Fig. 7c). It becomes evident that the garnets of samples ZLN 100, ZLN 86 and ZLN 72 show the highest Ca/(Mg + Ca + Fe + Mn) values, while those of majoritic garnets from samples ZLN 128, ZLN 141 and ZLN 124 (excluding ZLN 124 Chl) are significantly lower with a large spread in Mg/(Fe + Mn) ratios that decrease in the same order. Majoritic garnets of samples ZLN 116 and ZLN

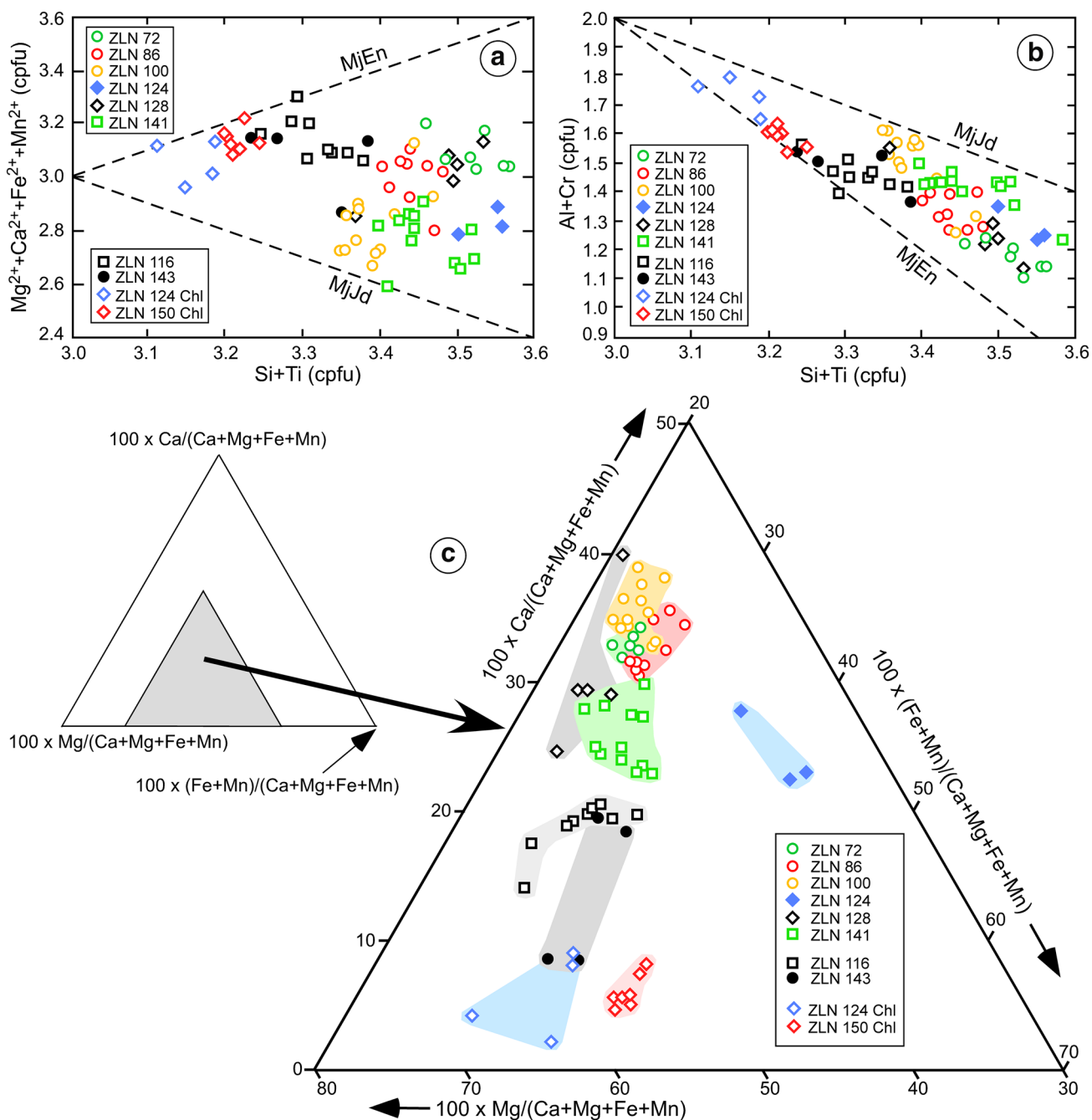


Fig. 7 Compositions of majoritic garnet grains formed in various shock-induced melt veins of amphibolites from the Ries. MjEn and MjJd are trendlines of the two substitution types occurring in majoritic garnets, i.e., $2 Al^{3+} = Si^{4+} + M^{2+}$ and $M^{2+} + Al^{3+} = Na^{+} + Si^{4+}$, respectively. While MjEn preferentially occurs in peridotite systems, MjJd is found in metabasalts that often show both substitution mechanisms (Kiseeva et al. 2013). **a** Total of M^{2+} cations vs Si + Ti (both in cations per formula unit (cpfu)). Majoritic garnets from different samples show different relative amounts of the two substitutions. **b**

Variation of Al + Cr (cpfu) vs Si + Ti (cpfu). Note that the majoritic garnets from the Ries again plot into the space between the two substitution lines. **c** Relative variation of divalent cations Ca, Mg and (Fe + Mn) (cpfu) in majoritic garnets from the Ries. Majoritic garnet grains of samples ZLN 72, ZLN 86, ZLN 100, ZLN 124, ZLN 128 and ZLN 141 show relatively high Ca contents with variable relative amounts of Mg and (Fe + Mn), while those of samples ZLN 124 Chl and ZLN 150 Chl show the lowest contents of Ca

143 show intermediate Ca/(Mg + Ca + Fe + Mn) values, while those that formed from melts rich in chlorite components (ZLN 124 Chl, ZLN 150 Chl) have the lowest values (Fig. 7c).

Discussion

Dependence of majoritic garnet composition on pressure and bulk composition

Majoritic garnets in the shock-induced melt veins show a large variation in both $^{VI}(\text{Si} + \text{Ti})$ (0.12–0.58 cpfu) and their relative concentrations of Ca, Mg and (Fe + Mn) (Table 2, Fig. 7c). These chemical variations may be caused by different P – T conditions of majoritic garnet formation and/or by different compositions of the melts from which these garnets crystallized.

An empirical barometer based on the variation of (Al + Cr) with Si in experimentally produced majoritic garnets (Stachel 2001) was used by Stähle et al. (2011) to estimate the P – T conditions at which the majoritic garnets from the Ries were formed. Using the compositions of majoritic garnets from three samples (ZLN 72, ZLN 86 and ZLN 100), Stähle et al. (2011) estimated formation pressures of ~15–17 GPa. At that time, however, considerable Na_2O contents of the majoritic garnet grains were not taken into account. Based on the compositions of experimentally produced majoritic garnet grains in chondritic, peridotitic, kimberlitic and basaltic systems from the literature, Collerson et al. (2010) gave an empirical barometer for such garnets, whereby the bulk composition was not taken into consideration. Wijbrans et al. (2016) performed a number of

experiments between 6 and 14.5 GPa in a range of bulk compositions in the system SiO_2 – Al_2O_3 – Cr_2O_3 – CaO – MgO with varying Cr/(Cr + Al) ratios and used additional experimental data from the literature to define two different geobarometer equations for majoritic garnets in peridotitic and eclogitic (basaltic) compositions. We used both, the barometer of Collerson et al. (2010) and the barometer for basaltic compositions by Wijbrans et al. (2016) to calculate formation pressures of all majoritic garnets from the Ries. The results obtained with both barometers are compared in Fig. 8. For most majoritic garnets, pressure values obtained with the barometer of Collerson et al. (2010) are higher than those obtained with the barometer for basaltic compositions of Wijbrans et al. (2016). In addition, we state that pressure values calculated for samples ZLN 72, ZLN 86 and ZLN 100 (Stähle et al. 2011) using the empirical geobarometer of Stachel (2001) are 0.6–1.8 GPa lower than those obtained by applying the barometer of Wijbrans et al. (2016). Average pressure values for each sample are given in Table 3. It is obvious that the samples can be divided into the three groups that have already been differentiated by the amount of $^{VI}(\text{Si} + \text{Ti})$ in their majoritic garnets and by the relative contribution of different pre-shock minerals (amphibole, plagioclase, chlorite or chloritized biotite) to the melt of their shock-induced veins (Fig. 7).

The variations of Si and (Al + Cr) with the pressure values calculated with the geobarometer of Wijbrans et al. (2016) are shown in Fig. 9a, b. Silicon (cpfu) correlates positively with pressure, while (Al + Cr) correlates negatively with P . There are, however, significant differences among samples that indicate similar pressures.

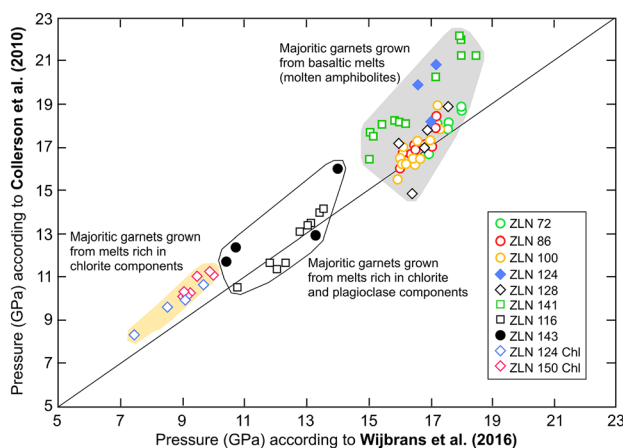


Fig. 8 Comparison of pressure values obtained with the majorite barometers of Collerson et al. (2010) and Wijbrans et al. (2016). For most majoritic garnets from the Ries higher pressure values are obtained with the barometer formulation of Collerson et al. (2010)

Table 3 Estimated crystallization pressures (averages) of majoritic garnets from the Ries

Sample no.	<i>n</i>	<i>P</i> (Wijbrans) (GPa)	<i>P</i> (Collerson) (GPa)
Majoritic garnet crystallized from amphibolitic melt			
ZLN 72	6	17.49 ± 0.40	18.06 ± 0.73
ZLN 86	9	16.67 ± 0.40	17.06 ± 0.40
ZLN 100	12	16.49 ± 0.47	16.83 ± 0.93
ZLN 124	3	16.96 ± 0.35	19.75 ± 0.95
ZLN 128	5	16.70 ± 0.53	17.08 ± 1.45
ZLN 141	12	16.54 ± 1.29	19.22 ± 1.91
Majoritic garnet grains crystallized from chloritic melt			
ZLN 150 Chl	7	9.43 ± 0.40	10.63 ± 0.50
ZLN 124 Chl	4	8.71 ± 0.88	9.62 ± 0.98
Majoritic garnet grains crystallized from mixed melts			
ZLN 116	9	12.58 ± 0.89	12.56 ± 1.27
ZLN 143	4	12.11 ± 1.78	13.26 ± 1.92

Pressures calculated with geobarometers of Wijbrans et al. (2016; metabasaltic rocks) and Collerson et al. (2010)

n number of analyses

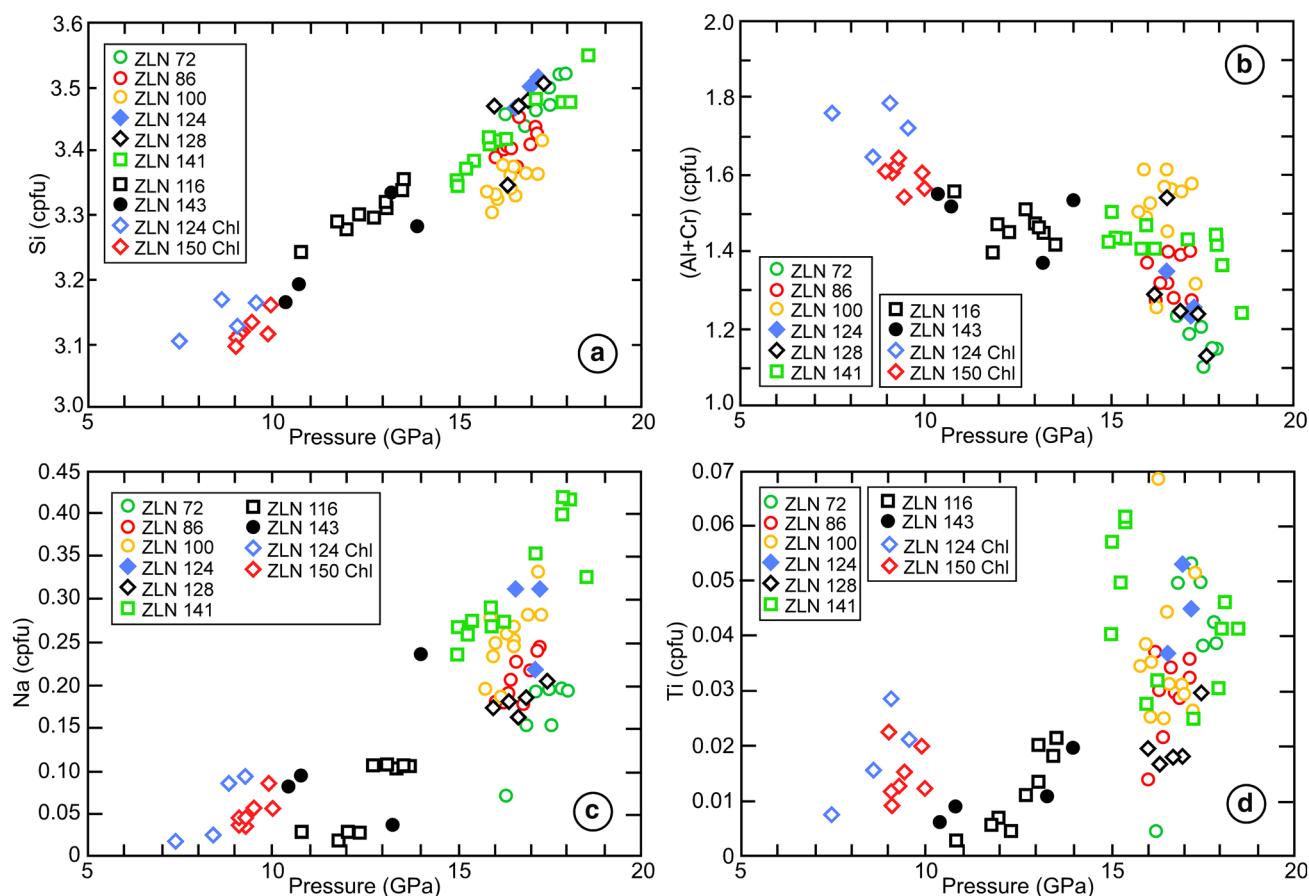


Fig. 9 Chemical composition of majoritic garnet from the Ries as a function of crystallization pressure calculated after Wijbrans et al. (2016). **a** Si (cpfu) shows a clear positive correlation with pressure. Note, however, that majoritic garnet grains from sample ZLN 100

show lower Si than those of sample ZLN 141. **b** Al + Cr (cpfu). Note that most majoritic garnets of sample ZLN 100 show higher values of (Al + Cr) (cpfu) than those of ZLN 141. **c** Na (cpfu). **d** Ti (cpfu)

For example, at the same pressure of 16.5 GPa majoritic garnets of sample ZLN 100 tend to show lower Si but higher (Al + Cr) than samples ZLN 72 and ZLN 86. Such differences are most probably caused by different chemical compositions of the shock-related melts from which these majoritic garnets crystallized. A final solution of this problem needs a lot more experimental data that may allow to clarify the dependence of majoritic garnet composition on variable bulk compositions at the same P – T conditions. Na and Ti show weak positive correlations with pressure (Fig. 9c, d).

Liquidus and solidus temperatures of variably composed shock-induced melt domains may be different. This means that during shock release and cooling, a relatively H_2O -poor or even dry basaltic melt may start to crystallize earlier, i.e., at higher pressure and temperature than a water-rich melt produced predominantly from chlorite.

Crystallization of majoritic garnet within the MORB system

Phase diagrams of dry and hydrous MORB up to 35 GPa and 2500 °C were discussed in detail by Litasov and Ohtani (2007) and a modified version of their diagram for dry MORB is given in Fig. 10a. At 17 GPa the liquidus of dry MORB is at 2170 °C and the solidus at 2080 °C. Note that at the solidus clinopyroxene (Cpx) is only stable up to 16.7 GPa. Below this pressure, the crystallization sequence in MORB is majoritic garnet followed by Cpx and stishovite (Sti).

Minor amounts of an unspecified Fe–Ti oxide phase may also be present at or below the solidus. At pressure values above 16.7 GPa, the crystallization sequence is just majoritic garnet followed by stishovite (\pm Fe–Ti oxide). In the ‘wet’ system (MORB + 2 wt% H_2O , not shown), the solidus

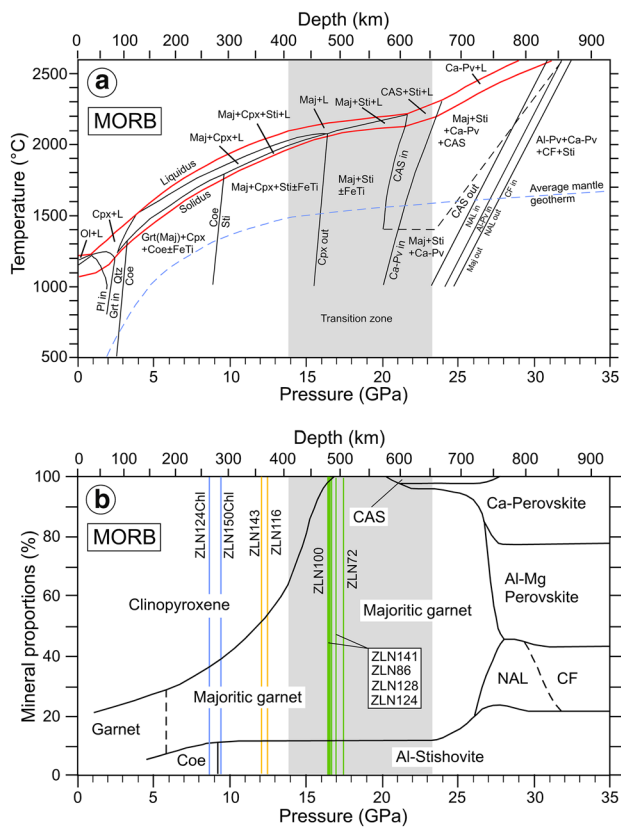


Fig. 10 **a** Phase diagram of anhydrous MORB deduced by Litasov and Ohtani (2007) from various experimental results. See text for discussion. *Al-Pv* Al-rich Mg-perovskite, *Ca-Pv* Ca-rich Mg-perovskite, *CF* Ca-ferrite type phase ($\text{NaAlSiO}_4\text{-MgAl}_2\text{O}_4$), *CAS* CAS phase ($\text{CaAl}_4\text{Si}_2\text{O}_{11}\text{-NaAl}_3\text{Si}_3\text{O}_{11}$), *Coe* coesite, *FeTi* Fe-Ti oxides, *Cpx* clinopyroxene, *Grt* garnet, *Maj* majoritic garnet, *NAL* Al-rich phase ($[\text{Na, K, Ca}][\text{Mg, Fe}^{2+}]_2[\text{Al, Fe}^{3+}, \text{Si}]_{5.5-6.0}\text{O}_{12}$), *Pl* plagioclase, *Ol* olivine, *Qtz* quartz, *Sti* stishovite. Note the average mantle geotherm. **b** Mineral proportions in dry MORB along an average geotherm (**a**) into deeper parts of the earth's mantle from Litasov and Ohtani (2007). Pressures (GPa) and correlated depths (km) are seen in the lower and upper horizontal line, respectively. Average pressures (Wijbrans et al. 2016) deduced for those majoritic garnets from the Ries that crystallized from amphibolite melts (green) are between 16.5 and 17.5 GPa and correspond to those of the upper transition zone (~480–510 km depth). Majoritic garnets that crystallized from chlorite melts (blue) formed later, at lower pressure values of ~9 GPa corresponding to a depth of ~275 km (upper mantle). It is assumed that majorites of the samples ZLN 116 and ZLN 143 (yellow) crystallized from melts with compositions between chlorite and bulk rock at pressure between 12 and 13 GPa. For abbreviations see **a**

at 17 GPa was estimated to be at ~1930 °C (Litasov and Ohtani 2007).

Subsolidus mineral proportions of the dry MORB system were estimated by Litasov and Ohtani (2007) using literature data (Fig. 10b). When the average pressure values obtained for the majoritic garnets from the various Ries samples (Table 3) using the geobarometer of Wijbrans et al. (2016) are transferred into this diagram they fall into the area of

the mantle transition zone and the lower parts of the upper mantle (Fig. 10b). Those majoritic garnets that crystallized from basaltic melts plot at depths where majoritic garnet and *Sti* are the principal minerals, perhaps accompanied by small amounts of *Cpx*. However, in the melt veins of shocked amphibolites ZLN 72, ZLN 86, ZLN 100, ZLN 116, ZLN 128 and ZLN 141, only glassy material (often transformed to clay minerals) instead of stishovite was found in the interstices of the majoritic garnets (Fig. 4a, b, d, e). This is certainly due to the marked instability of metastable stishovite, in particular at higher temperatures above ~500 or above 600 °C (Dachille et al. 1963; Gigl and Dachille 1968; Xue et al. 1993).

A *P-T-t* diagram for the evolution of shock-induced melt veins in amphibolites from suevite

As soon as a larger cosmic body impacts on a planetary surface two shock waves of supersonic speed will be created at the target–impactor interface. One will radiate into the target, while the other will spread outward towards the rear of the compressed impactor. When the latter wave arrives at the rear surface of the meteorite, this body will expand backwards and start to eject. At that moment, a rarefaction wave caused by pressure relief returns downwards following the preceding shock wave. However, the remoteness of the shock front ahead and the rarefaction wave behind diminish continuously because the rarefaction wave moves faster in the shock-compressed material and at some distance from the impact site, the rarefaction wave will capture the shock front and finally both waves become destroyed (French 1998; Collins et al. 2012; Langenhorst and Deutsch 2012).

The brief initial contact and compression stage (French 1998; Collins et al. 2012) ends when the rarefaction wave reaches the impactor–target interface. The duration of the time interval of maximum compression is given with $\tau_{cc} = L / (\nu_i \times \sin\theta)$, whereby L is the projectile diameter, ν_i corresponds to the impact velocity and $\sin\theta$ specifies the angle of incidence (Melosh 2013). A rough calculation for the Ries event with a projectile diameter of 1.5 km (Stöffler et al. 2002), a cosmic speed of 20 km s⁻¹ and an assumed inclined impact angle of ~49° results in 0.1 s duration for the initial peak continuum pressure. Shortly after, a shock wave with diminished continuum pressure in rocks far away from the impact site may produce locally high-temperature shear melts in the shape of erratically running shock veins.

During the last 20 years it came into practice to infer prevailing shock pressures in meteorites from the mineralogy of melt vein assemblages. First, Chen et al. (1996) claimed for the observed majoritic garnet + magnesio-wüstite assemblage in the Sixiangkou (L6) chondrite that this assemblage crystallized from melt at 2050–2300 °C and 20–24 GPa by comparing the phase stabilities with those in the Allende

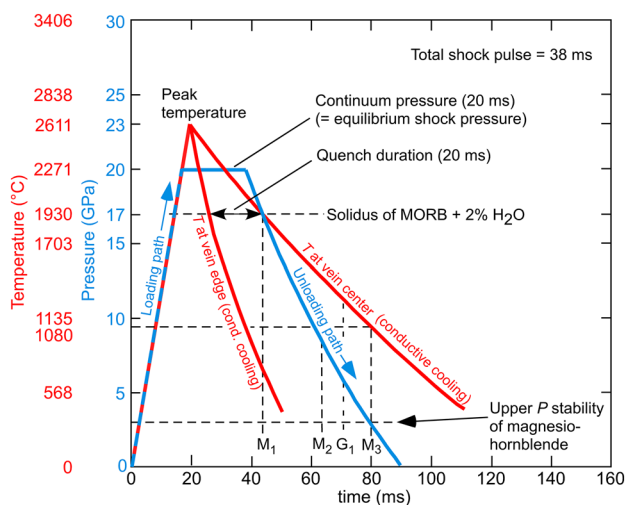


Fig. 11 Graphic diagram showing the P - T - t conditions of a typical shock vein (see Fig. 4f) in sample ZLN 128. The loading and unloading path (blue) of the shock wave is correlated with rising and falling temperatures (red) of the shear-induced shock vein. Conductive heat transfer to the cold host rock (~ 250 °C) triggers the fast cooling. Note that the vein edges cool faster than the vein center. The graphically ascertained peak temperature is 2611 °C. The solidus of the “MORB-type” melt (2 wt% H_2O) at 17 GPa lies at 1930 °C (Litasov and Ohtani 2007). The liquidus has not been determined but should lie about 90 °C higher. All majoritic garnets from amphibolitic melts must have crystallized at and above the solidus (M_1). Conductive cooling of the shock vein—most rapidly at the edge of the vein—fixes the quench time at the solidus in the ratio 1:9 (width of ‘glassy’ rim to half width of crystalline core, Fig. 4f). The continuum or equilibrium shock pressure (Xie et al. 2006a) close to it was fixed to 20 GPa, because higher pressures produce the CAS phase and/or Ca-perovskite as liquidus phases that were not observed in the Ries. The quench time span was assumed to be 20 ms (see Walton et al. 2016 for the reason). The majoritic garnets of chlorite provenance crystallized later (M_2) because the wet solidus at 9 GPa in the MASH system lies at ~ 1200 °C (Sumita and Inoue 1996). The partially shock-transformed hornblende fragment in sample ZLN 141 (Fig. 4c) determines the latest section of the falling temperatures and pressures. The glass around amphibole represents a residual melt after crystallization of significant amounts of majoritic garnet (G_1). The upper pressure stability of residual original hornblende in the core reaction structure (sample ZLN 128) lies at ~ 3 GPa and 1180 °C (M_3). The graphic diagram demonstrates that the dynamic event of the formation of a typical shock-induced vein lasts only about 100 ms

carbonaceous chondrite. The usefulness of this approach is underlined with similarity in texture, grain size and chemistry of the quench products in meteorites and static experiments (Sharp and DeCarli 2006).

It was emphasized by Sharp and DeCarli (2006) and Xie et al. (2006a) that UHP crystallisations in larger veins of meteorites should record the continuum shock pressure. To uncover the dynamic shock history of the veins and host rocks, these authors used time-controlled temperature and pressure profiles. Our proposed model for the P - T - t conditions of shock veins (Fig. 11) is based on a ~ 200 - μ m-thick melt vein in amphibolite ZLN 128 (Fig. 4f). The zoned vein

with largest majoritic garnets in the central domains reveals sequential crystallization. Small, ~ 10 - μ m-thick ‘glassy’ seams with fine crystallites at the edges demonstrate the beginning of a rapid quench due to conductive heat transfer into the shocked, but relatively cool host amphibolite rock (~ 250 °C, Stöffler and Grieve 2007). The majoritic garnets with largest grains (< 3 μ m) close to the center of the vein crystallized somewhat later and perhaps a little bit longer. However, any further crystallization stopped when the liquid passed the solidus (M_1 in Fig. 11).

Fast quenching of supercooled liquids provokes formation of large quantities of crystallites between the liquidus and solidus. At 17 GPa, a MORB liquid with 2 wt% H_2O has a solidus temperature of about 1930 °C (Litasov and Ohtani 2007). These data were inserted into a modeled diagram with an assumed continuum shock pressure of 20 GPa (Fig. 11). Higher shock pressures are not allowed since CAS and/or Ca-perovskite instead of majorite would be liquidus phases at rising pressures (Litasov and Ohtani 2007; Fig. 10a) and we neither observed CAS nor vitrified Ca-perovskite.

The rate at which a shock-induced melt vein quenches depends on both, the width of the vein and the temperature difference between the center of the vein and its host rock. Furthermore, the quench duration is related to the conductive heat transport from the vein to the host (Xie et al. 2006a). In the selected vein (Fig. 4f), the ratio of the width of the ‘glassy’ rim to that of the crystalline core is approximately one to nine and this ratio defines the time spans between (1) peak temperature and the time when the temperature at the vein edge reaches solidus temperature and (2) the time difference between the T curves for the edge and center of the vein at solidus temperature (Fig. 11). The peak temperature and the vein width force the timing of the conductive heat transfer. The assumed quench time of ~ 0.02 s in the diagram comes from thermal models of similar shock veins in meteorites (Walton et al. 2016). The graphical integration of the data into the modeled path of shock loading and unloading and the course of rising and falling temperatures results in our modelled P - T - t diagram (Fig. 11). The unknown peak temperature, which is mainly evoked from the shear-induced frictional heat is graphically extrapolated to 2611 °C.

The majoritic garnets of chlorite origin with the calculated crystallisation pressures of ~ 9 GPa lie in the P - T - t diagram far below the majoritic garnets that crystallized at ~ 17 GPa (Fig. 11). The wet solidus in the MASH system at 9 GPa corresponds to the temperature of ~ 1200 °C (Sumita and Inoue 1996). This means that the chlorite-derived majoritic garnets crystallized late in the dynamic event during pressure release (M_2 in Fig. 11). Thus, the garnets of chlorite origin are completely unrelated to the continuum shock pressures of their host rocks.

The hornblende fragment with a glassy intermediate zone (Fig. 4c) is an extraordinary object, which was only observed

in a shock vein of ZLN 141. Conductive heat emerging from the surrounding melt first caused marginal melting of the hornblende grain at high pressures. As pressure and temperature dropped, majoritic garnet grains started to crystallize from the cooler outside (Fig. 4c, d). During this crystallization, the melt thus changed its chemical composition and became relatively rich in SiO₂ and H₂O (Table 1; point G₁ in Fig. 11). The original unaltered amphibole crystal survived in the center of the fragment (Fig. 4c). During the last stage of shock unloading, the core of the hornblende fragment (Table 1) remained below the solidus at $P \approx 3$ GPa and $T \approx 1080$ °C (Niida and Green 1999) (point M₃ in Fig. 11). It must be emphasized that this extraordinary hornblende grain and its shock-related products document the whole time span of pressure release.

Non-majoritic garnets adjacent to shock veins

An assemblage of zoned garnet crystals (Si = 3.01–3.03 cpfu) occurs adjacent to the shock vein in ZLN 128 (Fig. 5c). It is assumed that the original garnet-bearing site was an area rich in secondary (pre-shock) chlorite surrounded by magnesio-hornblende (Mhb). Different brightness in BSE images uncover a distinct compositional zonation of the non-majoritic garnet grains (Fig. 5d, Table 1). The Ca–Mn-rich cores and Mg–Fe-rich rims of the garnet grains with sizes in the range of 2–10 µm formed during rapid growth at decreasing P – T conditions somewhat below 6 GPa (van Roermund and Drury 1998). Numerous magnetite inclusions mostly in concentric arrangement (Fig. 5d) manifest rising oxygen fugacities in the course of garnet formation. Breakdown of H₂O molecules and the escape of hydrogen (H₂) triggered increasing oxygen contents within the melt during the short phase of rapid cooling. The existence of non-majoritic garnet outside the shock vein suggests that these grains crystallized at a late stage, possibly at post-shock conditions. Similar Ca and Mn enrichments in the core (Type 1) characterize the most common zonation type of regional prograde metamorphic garnet.

Conclusions

Shock-induced veins in meteorites and terrestrial impact rocks are natural phenomena where various UHP phases and polymorphic mineral transitions occur. Their dynamic formation conditions in general are comparable with phase stabilities ascertained in laboratory static experiments. This report focuses on shock-induced veins within amphibolite fragments of shock stage 2 from Ries suevite. These weakly to moderately shocked rocks originated within the crystalline basement in distances of 1.7–2.1 km from the impact point (von Engelhardt et al. 1970). Their shock-induced

veins contain masses of majoritic garnet that were quenched from high-temperature frictional melts. Crystallization pressures were determined using new calculation methods of Collerson et al. (2010) and Wijbrans et al. (2016). Both geobarometers are (partially) based on the application of ^{VI}(Si + Ti) as well as Na contents, which are expressed in the structural formula of majoritic garnet. Fine shock veins with a maximal thickness of ~ 250 µm are confined to amphibolite rocks of shock stage 2a, whereas thicker veins up to 1100 µm in width occur exclusively in rock specimens of shock stage 2b.

The emphasis of this study lied on the decoding of the P – T – t conditions of the shock veins. On the basis of some time-dependent profiles (Sharp and DeCarli 2006; Xie et al. 2006a) shock-induced veins in nature can be graphically modelled with a high-angle loading and a steep-sloped unloading path (Fig. 11). The graphical design clearly demonstrates the magnitude of the short-lived shock pulse (time span between the shock front and the arrival of the release wave). This dynamic parameter is linked with the peak equilibrium pressure, which was created primarily at the impact site.

Main results and some new findings within the vein-bearing suevite clasts of the Ries are:

1. The recalculation of earlier analyses (Stähle et al. 2011) with the new geobarometer of Wijbrans et al. (2016) resulted in pressure values that are about 0.6–1.5 GPa higher than originally proposed. In total, 71 chemical analyses of majoritic garnet grains (Table 2 and Electronic Supplementary Material) in differently sized melt veins resulted in a great variety of ultrahigh pressure values in the range of ~ 8–18 GPa (Table 2; Fig. 8).
2. Three genetic types of majoritic garnet exist in shocked rocks of the Ries. The first one occurs in larger shock veins where the melts had (nearly) basaltic compositions (i.e., relatively rich in Na and Ca). The second type of majoritic garnet is of chlorite provenance and crystallized in thin melt veins which exclusively run parallel to chlorite-filled cracks. Careful inspection supports the impression that, when present, the veins follow former fractures. The third type with intermediate compositions resulted from melts derived primarily from chlorite and plagioclase.
3. To the best of our knowledge, amphibolite-derived majoritic garnet in the Ries is richest in Na and shows the highest calculated crystallisation pressure values, which were ever found in terrestrial rocks. These “MORB-type” majoritic garnets contain up to 2.99 wt% Na₂O and exhibit ultrahigh pressures in the range of 15–18 GPa (Table 2, Fig. 9c). The majoritic garnet no. 63 in ZLN 141 shows the largest excess amount of ^{VI}(Si + Ti) (0.58 cpfu) of all analyses (Table 2; Fig. 9)

indicating the presence of a large fraction of the two majorite components. In marked contrast, the chlorite-derived majoritic garnet grains were formed at lower pressures of about 9–13 GPa. Both types of majoritic garnet may occur in shock-induced veins of the same sample, as shown by ZLN 124. Therefore, majoritic garnets of chlorite (+ plagioclase) provenance cannot be used for the estimation of the continuum pressures due to low liquidus and solidus temperatures.

4. Graphically modelled P – T – t conditions of a 200- μm -wide shock vein in ZLN 128 (Fig. 4f) resulted in a peak temperature of ca. 2600 °C (Fig. 11). The large temperature gradient of more than 2300 °C from the hot melt to the cool shocked host rock at ca. 250 °C is remarkable. All types of majorites crystallized during pressure release, but the quenched ‘MORB-type’ majorite garnets formed close to the equilibrium pressure. Their existence in basic melt veins demonstrates shock pressures in the range of 15–18 GPa for the amphibolite clast ZLN 128 of shock stage 2b. The duration of the graphically established shock pulse (~ 38 ms) is roughly a third of the duration of the peak equilibrium pressure, which was produced primarily at the impact site.
5. A spectacular shock-induced feature is manifested in a glass-bearing amphibole fragment with majoritic margins (Fig. 4c) documenting the whole unloading path.

Summarizing we state that static experiments revealed that pyroxenes (MgSiO_3 , $\text{CaMgSi}_2\text{O}_6$, $\text{NaAlSi}_2\text{O}_6$) are totally solved in majoritic garnets above a pressure of ~ 17 GPa (Ringwood and Major 1966; Ringwood 1967; Akaogi and Akimoto 1977; Irifune et al. 1986; Akaogi et al. 1987; Irifune 1987). The majoritic garnet grains of sample ZLN 141 with the highest crystallisation pressure values (~ 18.5 GPa) would be stable at a mantle depth of ~ 500 km (Fig. 10). It is fascinating that the experimental results are realized in the existence of high-pressure phases and mineral transitions in shock-induced veins of the Ries crater, that is, in natural shocked samples lying on the Earth’s surface.

Acknowledgements We thank Klaus Tschira Stiftung for support. Our thanks are also due to Ilona Fin and Oliver Wienand for preparing excellent polished thin sections and to Johannes Grimm and Hans-Peter Meyer for their assistance with EPMA analyses. Furthermore, we are grateful to Richard Norris for critical reading of the manuscript and helpful remarks. Careful reviews by Othmar Müntener and two anonymous reviewers are gratefully acknowledged.

References

Akaogi M, Akimoto S (1977) Pyroxene–garnet solid-solution equilibria in the systems $\text{Mg}_4\text{Si}_4\text{O}_{12}$ – $\text{Mg}_3\text{Al}_2\text{Si}_3\text{O}_{12}$ and $\text{Fe}_4\text{Si}_4\text{O}_{12}$ – $\text{Fe}_3\text{Al}_2\text{Si}_3\text{O}_{12}$ at high pressures and temperatures. *Phys Earth Planet Inter* 15:90–106

- Akaogi M, Navrotsky A, Yagi T, Akimoto S (1987) Pyroxene–garnet transformation: thermochemistry and elasticity of garnet solid solutions, and application to a pyrolite mantle. In: Manghnani MH, Syono Y (eds) High-pressure research in mineral physics. Terra Scientific Publishing Company (TERRAPUB), Tokyo, pp 251–260
- Bindi L, Dymshits AM, Bobrov AV, Litasov KD, Shatsky AF, Ohtani E, Litvin YA (2011) Crystal chemistry of sodium in the Earth’s interior: the structure of $\text{Na}_2\text{MgSi}_5\text{O}_{12}$ synthesized at 17.5 GPa and 1700 °C. *Am Mineral* 96:447–450
- Biren MB, Spray JG (2011) Shock veins in the central uplift of the Manicouagan impact structure: context and genesis. *Earth Planet Sci Lett* 303:310–322
- Bobrov AV, Kojitani H, Akaogi M, Litvin YA (2008) Phase relations on the diopside–jadeite–hedenbergite join up to 24 GPa and stability of Na-bearing majoritic garnet. *Geochim Cosmochim Acta* 72:2392–2408
- Bobrov AV, Dymshits AM, Litvin YA (2009) Conditions of magmatic crystallization of Na-bearing majoritic garnets in the earth mantle: evidence from experimental and natural data. *Geochem Int* 47:951–965
- Bromiley GD, Bromiley FA, Bromiley DW (2006) On the mechanisms for H and Al incorporation in stishovite. *Phys Chem Miner* 33:613–621
- Buchner E, Schmieder M, Schwarz WH, Trierloff M (2013) Das Alter des Meteoritenkraters Nördlinger Ries—eine Übersicht und kurze Diskussion der neueren Datierungen des Riesimpakts. *Z Dtsch Ges Geowiss* 164:433–445
- Chao ECT (1967) Shock effects in certain rock-forming minerals. *Science* 156:192–202
- Chao ECT, Hüttner R, Schmidt-Kaler H (1978) Principal exposures of the Ries meteorite crater in southern Germany. *Bayer Geol Landesamt, München*, p 84
- Chen M, Sharp TG, El Goresy A, Wopenka B, Xie X (1996) The majorite–pyrope plus magnesiowüstite assemblage: constraints on the history of shock veins in chondrites. *Science* 271:1570–1573
- Chung JI, Kagi H (2002) High concentration of water in stishovite in the MORB system. *Geophys Res Lett* 29:2020. doi:10.1029/2002GL015579
- Collerson KD, Williams Q, Kamber BS, Omori S, Arai H, Ohtani E (2010) Majoritic garnet: a new approach to pressure estimation of shock events in meteorites and the encapsulation of sublithospheric inclusions in diamond. *Geochim Cosmochim Acta* 74:5939–5957
- Collins GS, Melosh HJ, Osinski GR (2012) The impact-cratering process. *Elements* 8:25–30
- Dachille F, Zeto RJ, Roy R (1963) Coesite and stishovite: stepwise reversal transformations. *Science* 140:991–993
- Dressler B, Graup G (1970) Pseudotachylite aus dem Nördlinger Ries, 2nd edition. *Geol Bavar* 61:201–228
- Dressler B, Graup G, Matzke K (1969) Die Gesteine des kristallinen Grundgebirges im Nördlinger Ries. *Geol Bavar* 61:201–228
- Dubrovinsky LS, El Goresy A, Gillet P, Wu X, Simionovici A (2009) A novel natural shock-induced high-pressure polymorph of FeTiO_3 ilmenite with the Li-niobate structure from the Ries crater, Germany. *Meteorit Planet Sci* 44(S7):Abstract A64
- Dymshits AM, Bobrov AV, Bindi L, Litvin YA, Litasov KD, Shatskiy AF, Ohtani E (2013) Na-bearing majoritic garnet in the $\text{Na}_2\text{MgSi}_5\text{O}_{12}$ – $\text{Mg}_3\text{Al}_2\text{Si}_3\text{O}_{12}$ join at 11–20 GPa: phase relations, structural peculiarities and solid solutions. *Geochim Cosmochim Acta* 105:1–13
- El Goresy A, Chen M, Gillet P, Dubrovinsky L, Graup G, Ahuja R (2001) A natural shock-induced dense polymorph of rutile with α - PbO_2 structure in the suevite from the Ries crater in Germany. *Earth Planet Sci Lett* 192:485–495

- El Goresy A, Dubrovinsky L, Gillet P, Graup G, Chen M (2010) Akaogiite: an ultra-dense polymorph of TiO_2 with the baddeleyite-type structure, in shocked garnet gneiss from the Ries Crater, Germany. *Am Mineral* 95:892–895
- El Goresy A, Gillet P, Miyahara M, Ohtani E, Ozawa S, Beck P, Montagnac G (2013) Shock-induced deformation of shergottites: shock-pressures and perturbations of magmatic ages on Mars. *Geochim Cosmochim Acta* 101:233–262
- French BM (1998) Traces of a catastrophe: a handbook of shock-metamorphic effects in terrestrial meteorite impact structures. LPI Contribution No. 954 Lunar and Planetary Institute, 120 p
- French BM, Koeberl C (2010) The convincing identification of terrestrial meteorite impact structures: what works, what doesn't, and why. *Earth Sci Rev* 98:123–170
- French BM, Short NM (1968) Shock metamorphism of natural materials. Mono Book Corp, Baltimore, p 644
- Gigl PD, Dachille F (1968) Effect of pressure and temperature on the reversal transitions of stishovite. *Meteoritics* 4:123–136
- Gillet P, El Goresy A (2013) Shock events in the solar system: the message from minerals in terrestrial planets and asteroids. *Annu Rev Earth Planet Sci* 41:257–285
- Gillet P, El Goresy A, Beck P, Chen M (2007) High-pressure mineral assemblages in shocked meteorites and shocked terrestrial rocks: mechanisms of phase transformations and constraints to pressure and temperature histories. In: Ohtani E (ed) *Advances in high-pressure mineralogy*. Geol Soc Amer Spec, Boulder, pp 57–82
- Graup G (1977) Die Petrographie der kristallinen Gesteine der Forschungsbohrung Nördlingen 1973. *Geol Bavar* 75:219–229 (Paper 421)
- Graup G (1978) Das Kristallin im Nördlinger Ries Petrographische Zusammensetzung und Auswurfmechanismus der kristallinen Trümmernmassen, Struktur des kristallinen Untergrundes und Beziehungen zum Moldanubikum. Enke Verlag, Stuttgart, p 190
- Harte B (2010) Diamond formation in the deep mantle: the record of mineral inclusions and their distribution in relation to mantle dehydration zones. *Mineral Mag* 74:189–215
- Hawthorne FC, Oberti R, Harlow GE, Maresch WV, Martin RF, Schumacher JC, Welch MD (2012) IMA report, nomenclature of the amphibole supergroup. *Am Mineral* 97:2031–2048
- Hüttner R, Schmidt-Kaler H (1999) Wanderungen in der Erdgeschichte—Meteoritenkrater Nördlinger Ries, vol 10. Verlag F. Pfeil, München, p 144
- Irfune T (1987) An experimental investigation of the pyroxene-garnet transformation in a pyrolyte composition and its bearing on the constitution of the mantle. *Phys Earth Planet Inter* 45:324–336
- Irfune T, Sekine T, Ringwood AE, Hibberson WO (1986) The eclogite-garnetite transformation at high pressure and some geophysical implications. *Earth Planet Sci Lett* 77:245–256
- James OB (1969) Jadeite: shock-induced formation from oligoclase, Ries crater, Germany. *Science* 165:1005–1008
- Kenkmann T, Ivanov BA (2006) Target delamination by spallation and ejecta dragging: an example from the Ries crater's periphery. *Earth Planet Sci Lett* 252:15–29
- Kiseeva ES, Yaxley GM, Stepanov AS, Tkalčić H, Litasov KD, Kamenetsky VS (2013) Metapyroxenite in the mantle transition zone revealed from majorite inclusions in diamonds. *Geology* 41:883–886
- Kiseeva ES, Wood BJ, Ghosh S, Stachel T (2016) The pyroxenite–diamond connection. *Geochem Perspect Lett* 2:1–9
- Lambert P (1981) Breccia dikes: geological constraints on the formation of complex craters. In: *Multi-ring basins. Formation and evolution. Proceedings of the lunar and planetary science conference*, pp 59–78
- Lambert P (2010) Target and impact deposits at Rochechouart impact structure, France. *Geol Soc Am Spec* 465:509–541
- Langenhorst F, Deutsch A (2012) Shock metamorphism of minerals. *Elements* 8:31–36
- Langenhorst F, Dressler B (2003) First observation of silicate hollandite in a terrestrial rock. In: *Large meteorite impacts. Lunar Planetary Institute contribution No. 1167, Abstract 4046*
- Langenhorst F, Poirier JP, Deutsch A, Hornemann U (2002) Experimental approach to generate shock veins in single crystal olivine by shear melting. *Meteorit Planet Sci* 37:1541–1553
- Liou JG, Tsujimori T, Yang J, Zhang RY, Ernst WG (2014) Recycling of crustal materials through study of ultrahigh-pressure minerals in collisional orogens, ophiolites, and mantle xenoliths: a review. *J Asian Earth Sci* 96:386–420
- Litasov KD, Ohtani E (2005) Phase relations in hydrous MORB at 18–28 GPa: implications for heterogeneity of the lower mantle. *Phys Earth Planet Inter* 150:239–263
- Litasov KD, Ohtani E (2007) Effect of water on the phase relations in earth's mantle and deep water cycle: advances in high-pressure mineralogy. *Geol Soc Am Spec* 421:115–156
- Litasov KD, Kagi H, Shatskiy A, Ohtani E, Lakshtanov DL, Bass JD, Ito E (2007) High hydrogen solubility in Al-rich stishovite and water transport in the lower mantle. *Earth Planet Sci Lett* 262:620–634
- Liu X, Nishiyama N, Sanchira T, Inoue T, Higo Y, Sakamoto S (2006) Decomposition of kyanite and solubility of Al_2O_3 in stishovite at high pressure and high temperature conditions. *Phys Chem Miner* 33:711–721
- Liu L, Zhang J, Green HW II, Jin Z, Bozhilov KN (2007) Evidence of former stishovite in metamorphosed sediments, implying subduction to > 350 km. *Earth Planet Sci Lett* 263:180–191
- Martini JEJ (1978) Coesite and stishovite in the Vredefort Dome, South Africa. *Nature* 272:715–717
- Martini JEJ (1991) The nature, distribution and genesis of the coesite and stishovite associated with the pseudotachylite of the Vredefort Dome, South Africa. *Earth Planet Sci Lett* 103:285–300
- Melosh HJ (2013) The contact and compression stage of impact cratering. In: Osinski GR, Pierazzo E (eds) *Impact cratering: processes and products*. Blackwell, Oxford, pp 32–42
- Miyahara M, Ohtani E, Yamaguchi A, Ozawa S, Sakai T, Hirao N (2014) Discovery of coesite and stishovite in eucrite. *PNAS* 111:10939–10942
- Nasdala L, Reiners PW, Garver JJ, Kennedy AK, Stern RA, Balan E, Wirth R (2004) Incomplete retention of radiation damage in zircon from Sri Lanka. *Am Mineral* 89:219–231
- Niida K, Green DH (1999) Stability and chemical composition of paragonitic amphibole in MORB pyrolyte under upper mantle conditions. *Contrib Mineral Petrol* 135:18–40
- Ono S, Yasuda A (1996) Compositional change of majoritic garnet in a MORB composition from 7 to 17 GPa and 1400 to 1600 °C. *Phys Earth Planet Inter* 96:171–179
- Panero WR (2006) Aluminium incorporation in stishovite. *Geophys Res Lett* 33:L20317. doi:10.1029/2006GL027425
- Panero W, Benedetti L, Jeanloz R (2003) Transport of water into the lower mantle: role of stishovite. *J Geophys Res Solid Earth* 108:2039. doi:10.1029/2002JB002053
- Pohl J, Stöffler D, Gall H, Ernstson K (1977) The Ries impact crater. In: Roddy DJ, Pepin RO, Merrill RB (eds) *Impact and explosion cratering*. Pergamon Press, New York, pp 343–404
- Ringwood AE (1967) The pyroxene-garnet transformation in the earth's mantle. *Earth Planet Sci Lett* 2:255–263
- Ringwood AE, Major A (1966) High-pressure transformations in pyroxenes. *Earth Planet Sci Lett* 1:351–357
- Ringwood AE, Major A (1971) Synthesis of majorite and other high pressure garnets and perovskites. *Earth Planet Sci Lett* 12:411–418
- Rocholl A, Ovtcharova M, Schaltegger U, Wijbrans J, Pohl J, Harzhauser M, Prieto J, Ulbig A, Boehme M (2011) A precise and

- accurate “astronomical” age of the Ries impact crater, Germany: a cautious note on argon dating of impact material. *Geophys Res* 13:13322–13327 (**Abstracts 13: EGU2011, EGU General Assembly 2011**)
- Schmidt-Kaler H, Treibs W, Hüttner R (1970) *Exkursionsführer zur geologischen Übersichtskarte des Rieses 1:100 000*. Bayer Geol Landesamt, München, p 68
- Schwarz WH, Lippolt HJ (2014) ^{40}Ar – ^{39}Ar step-heating of impact glasses from the Nördlinger Ries impact crater—Implications on excess argon in impact melts and tektites. *Meteorit Planet Sci* 49:1023–1036
- Sharp TG, DeCarli PS (2006) Shock effects in meteorites. In: Lauretta DS, McSween HY Jr (eds) *Meteorites and the early solar system II*. University Arizona Press, Tucson, pp 653–677
- Spray JG (1998) Localized shock-and friction-induced melting in response to hypervelocity impact. In: Grady MM, Hutchinson R, McCall GJH, Rothery DA (eds) *Meteorites: flux with time and impact effects*. Geol Soc SP 140, London, pp 195–204
- Spray JG, Kelley SP, Rowley DB (1998) Evidence for a late triassic multiple impact event on earth. *Nature* 392:171–173
- Spray A, Butler HR, Thompson LM (2004) Tectonic influences on the morphometry of the sudbury impact structure: implications for terrestrial cratering and modeling. *Meteorit Planet Sci* 39:287–301
- Spry A (1969) *Metamorphic textures*. Pergamon Press, Oxford, p 350
- Stachel T (2001) Diamonds from the asthenosphere and the transition zone. *Eur J Mineral* 13:883–892
- Stähle V (1973) Cordierite glass formed by shock in a cordierite-garnet-gneiss from the Ries crater, Germany. *Earth Planet Sci Lett* 18:385–390
- Stähle V, Altherr R, Koch M, Nasdala L (2004) Shock-induced formation of kyanite (Al_2SiO_5) from sillimanite within a dense metamorphic rock from the Ries crater (Germany). *Contrib Mineral Petrol* 148:150–159
- Stähle V, Altherr R, Koch M, Nasdala L (2008) Shock-induced growth and metastability of stishovite and coesite in lithic clasts from suevite of the Ries impact crater (Germany). *Contrib Mineral Petrol* 155:457–472
- Stähle V, Altherr R, Nasdala L, Ludwig T (2011) Ca-rich majorite derived from high-temperature melt and thermally stressed hornblende in shock veins of crustal rocks from the Ries impact crater (Germany). *Contrib Mineral Petrol* 161:275–291
- Stettner G (1974) Das Grundgebirge in der Forschungsbohrung Nördlingen 1973 im regionalen Rahmen und seine Veränderungen durch den Impakt. *Geol Bavar* 72:35–51
- Stöffler D (1972) Deformation and transformation of rock-forming minerals by natural and experimental shock processes. I. Behavior of minerals under shock compression. *Fortschr Mineral* 49:50–113
- Stöffler D, Grieve RAF (2007) Impactites. In: Fettes D, Desmons J (eds) *Metamorphic rocks: a classification and glossary of terms, Recommendations of the International Union of Geological Sciences. Subcommission on the Systematics of Metamorphic Rocks*. Cambridge University Press, Cambridge, pp 82–92
- Stöffler D, Keil K, Scott ERD (1991) Shock metamorphism of ordinary chondrites. *Geochim Cosmochim Acta* 55:3845–3867
- Stöffler D, Artemieva NA, Pierazzo E (2002) Modeling the Ries–Steinheim impact event and the formation of the moldavite strewn field. *Meteorit Planet Sci* 37:1893–1907
- Stöffler D, Artemieva NA, Wünnemann K, Reimold WU, Jacob J, Hansen BK, Summerson IAT (2013) Ries crater and suevite revisited—observations and modeling Part I: observations. *Meteorit Planet Sci* 48:515–589
- Sumita T, Inoue T (1996) Melting experiments and thermodynamic analyses on silicate– H_2O systems up to 12 GPa. *Phys Earth Planet Inter* 96:187–200
- Tomioka N, Miyahara M (2017) High-pressure minerals in shocked meteorites. *Meteorit Planet Sci* 52:1–23. doi:10.1111/maps.12902
- Tschauner O, Ma C (2017) Riesite, IMA 2015-110a. CNMNC Newsletter No. 35, February 2017: p 213. *Mineral Mag* 81:209–213
- Tschauner O, Ma C, Lanzirotti A, Newville M (2017) Riesite, a new high pressure polymorph of TiO_2 that forms upon shock-release—comparison to $(\text{Zr}, \text{Ti})\text{O}_2$ in pseudotachylites. Abstract Goldschmidt Conference 2017
- van Roermund HLM, Drury MR (1998) Ultra-high pressure ($P > 6$ GPa) garnet peridotites in Western Norway: exhumation of mantle rocks from > 185 km depth. *Terra Nova* 10:295–301
- von Engelhardt W, Stöffler D, Schneider W (1970) *Petrologische Untersuchungen im Ries*, 2nd edition. *Geol Bavar* 61:229–295
- Walton EL, Sharp TG, Hu J (2016) Frictional melting processes and the generation of shock veins in terrestrial impact structures: evidence from the Steen River impact structure, Alberta, Canada. *Geochim Cosmochim Acta* 180:256–270
- Wijbrans CH, Rohrbach A, Klemme S (2016) An experimental investigation of the stability of majoritic garnet in the earth’s mantle and an improved majorite geobarometer. *Contrib Mineral Petrol* 171:50
- Xie Z, Sharp TG, DeCarli PS (2006a) Estimating shock pressures based on high-pressure minerals in shock-induced melt veins of L chondrites. *Meteorit Planet Sci* 41:1883–1898
- Xie Z, Sharp TG, DeCarli PS (2006b) High-pressure phases in a shock-induced melt vein of the Tenham L6 chondrite: constraints on shock pressure and duration. *Geochim Cosmochim Acta* 70:504–515
- Xue X, Stebbins JF, Kanzaki M (1993) A ^{29}Si MAS NMR study of sub-Tg amorphization of stishovite at ambient pressure. *Phys Chem Miner* 19:480–485